Synaptic distribution of individually labeled mitral cells in the external plexiform layer of the mouse olfactory bulb

Takeshi Matsuno[1], Emi Kiyokage[1], Kazunori Toida[1, 2]*

[1]Department of Anatomy, Kawasaki Medical School,
577 Matsushima, Kurashiki, Okayama, 701-0192, Japan
[2]Research Center for Ultra-High Voltage Electron Microscopy,
Osaka University, Osaka, 567-0047, Japan

48 text pages, 13 figures and 2 tables in 15 plates, 57 references

Abbreviated title: Synaptic distribution on mitral cells

Associate editor: Professor Thomas Finger

Keywords: synapse, dendrites, parvalbumin, gephyrin, electron microscopy, Sindbis viral vector, nif-0000-10294, SCR_007370, SCR_013672, AB_11180610, AB_2336890, AB_2187695, AB_2301998, AB_10000345, AB_887717

***Corresponding author:** Kazunori Toida, M.D., Ph.D.
Professor and Chairman, Department of Anatomy,
Kawasaki Medical School,
577 Matsushima, Kurashiki, Okayama, 701-0192, Japan.
Tel.: +81 (86)-462-1111, Ext. 27520
Fax: +81 (86)-462-1199
E-mail: toida@med.kawasaki-m.ac.jp

Grant support: MEXT/JSPS KAKENHI Grant JP15K06748; Grant JP24500418; Grant JP23500419. Research Project Grant from Kawasaki Medical School; Grant number 26B-88; Grant number 26B-43; Grant number 26G-6

Abstract

Mitral cells are the major projection neurons of the olfactory bulb. They receive olfactory inputs, regulate information, and project their axons to the olfactory cortex. To better understand output regulation of mitral cells, we established a method to visualize individual projection neurons and quantitatively examined their synaptic distribution. Individual mitral cells were labeled by viral injection, 3D-reconstructed with light microscopy, and serial-sectioned for electron microscopy. Synaptic distributions were analyzed in electron microscopically reconstructed cell bodies, two regions of secondary dendrites (near the somata and ≈ 200 μm from the somata), and primary dendrites. The ratio of presynaptic sites (60%) and reciprocal synapses (60% presynaptic and 80% postsynaptic sites) were similar in each region. Characteristically, primary dendrite synapses were mainly distributed within the inner half of the external plexiform layer (EPL). For comparison, tufted cells were also examined, and the synaptic distribution in two secondary dendrite regions, which corresponded with mitral cells, was analyzed. Results showed that the ratio of reciprocal synapses (80% presynaptic and 90% postsynaptic sites) was greater than in mitral cells. The distribution of symmetrical synapses was also analyzed using synaptic and neuronal markers, such as parvalbumin, vesicular gamma-aminobutyric acid transporter, and gephyrin. Parvalbumin-expressing neurons tended to form synapses on secondary dendrites near the somata and were more uniformly distributed on primary dendrites of mitral cells. These results indicated that local mitral cell synaptic circuits are formed in accordance with their functional roles and restricted to the inner half of the EPL.

ABBREVIATIONS

(+): immunoreactive

(-): immunonegative

ABC: avidin-biotin peroxidase complex

BSA: bovine serum albumin

DAB: 3, 3'-diaminobenzidine tetrahydrochloride

EM: electron microscopy

EPL: external plexiform layer

GABA: gamma-aminobutyric acid

GFP: green fluorescent protein

GL: glomerular layer

MCL: mitral cell layer

mRFP: monomeric red fluorescent protein

OB: olfactory bulb

palGFP: palmitoylation site-attached green fluorescent protein

palmRFP: palmitoylation site-attached monomeric red fluorescent protein

PB: phosphate buffer

PBS: phosphate buffered saline

PV: parvalbumin

VGAT: vesicular GABA transporter

VGLUT1: vesicular glutamate transporter 1

Introduction

The olfactory bulb (OB) is the primary center of the olfactory system in the brain, where odor information that is transferred from olfactory receptor neurons is integrated, processed, and transmitted to higher brain regions (Mori et al., 1999).

Mitral cells, which are the major projection neurons of the OB, extend their primary dendrites into single glomeruli, receive inputs from olfactory sensory neurons at intraglomerular dendritic tufts, and project axons to the olfactory cortex (Price and Powell, 1970). Mitral cells also give rise to secondary dendrites from their cell bodies, and these dendrites horizontally extend deep into the external plexiform layer (EPL). Dendritic tufts and secondary dendrites of mitral cells form characteristic synapses, known as “reciprocal synapses,” with interneurons. The reciprocal synapses consist of a presynaptic site of an asymmetrical synapse from mitral/tufted cells to interneurons and a postsynaptic site of a symmetrical synapse reciprocally from interneurons to mitral/tufted cells, which are located side by side between the same neurons (Price and Powell, 1970). The reciprocal synapses formed on dendritic tufts and secondary dendrites are thought to play a role in olfactory input processing of information transferred to the soma (Kosaka et al., 1995, 1997; Aungst et al., 2003) and regulation of olfactory output, respectively, before projecting to the olfactory cortex (Yokoi et al. 1995; Mori et al., 1999; Miyamichi et al., 2013).

In the EPL, at least two types of gamma-aminobutyric acid (GABA)ergic interneurons form reciprocal synapses with mitral cells—granule cells and neurons immunoreactive for parvalbumin (PV(+)). In our previous studies, we showed that synaptic distribution on PV(+) neurons formed with presumed mitral/tufted cells, and processes of presumed mitral/tufted cells formed with PV(+) neurons and granule cells (Toida et al., 1994, 1996,

Toida 2008). We also showed that approximately 90% of synapses on granule cells form reciprocal synapses, and around 30% of synapses on PV(+) neurons form reciprocal synapses. However, the areas where synaptic distribution on individual mitral cells has been analyzed remain limited. Mitral cells are adjacent to other secondary dendrites that broadly extend, and intermingle with each other or with other neuronal profiles in the EPL. Although high-resolution analysis by electron microscopy (EM) enables synapse identification, the sample area for analysis remains somewhat limited, and there is a need for selective markers that label individual mitral cells for efficient EM analysis of synaptic distribution. Golgi staining and intracellular injection are useful tools for extensive labeling of neurons (Ramón y Cajal et al., 1904; Mori et al., 1983; Orona et al., 1984), but these methods have limitations when applied to subsequent correlative EM studies. Recent methods for selectively labeling individual neurons with viral vectors have been developed for correlative EM applications. Among them, the Sindbis virus is particularly useful for selective labeling of projection neurons (Furuta et al., 2001; Suzuki et al., 2015); in our hands, this viral vector was an effective tool for analyzing detailed distribution of synapses on mitral cells. The analysis of synaptic distribution of mitral cells that interact with interneurons will provide a better understanding of the characteristics of local circuits in the EPL, as well as the mechanisms of processing perceptual information in the OB.

In this study, our aim was to analyze precise mitral cell synaptic distributions by establishing a method to visualize individual mitral cells using a Sindbis viral vector. These results are expected to help identify the morphological basis of odor information processing.

Materials and Methods

Animals and fixation

A total of 49 male and nine female C57BL/6J mice (8–10 weeks old, weighing 20–25 g from Japan SLC, Inc., Shizuoka, Japan) were used in this study. We used 20 male and nine female mice for 3D reconstruction, two male mice and one female mouse for serial EM studies, and 10 male mice and one female mouse for correlative confocal laser microscopy and EM studies. We used 18 male mice for analysis of synaptic distributions using Imaris 7.7.2 software (Bitplane, Saint Paul, MN, USA; RRID:SCR_007370), as described below. All animal experiments were approved by the Animal Research Committee of Kawasaki Medical School (approval #13-034) and performed according to the "Guide for Care and Use of Laboratory Animals" of Kawasaki Medical School. The mice were deeply anesthetized with sodium pentobarbital (100 mg/kg body weight), and fixed via transcardial perfusion with a mixture of 4% paraformaldehyde and 1% glutaraldehyde in 0.1 M phosphate buffer (PB, pH 7.4). Brains were removed from the skull and immersed in the same fixative for 1 day at 4°C. The OBs were resected from the rest of the brains and cryoprotected with 30% sucrose in 0.1 M PB for 3–6 hours. The OBs were frozen in liquid nitrogen for 10–15 seconds and thawed in 0.1 M PB, followed by serial sectioning into 50-μm-thick coronal sections on a microtome (VT 1200S, Leica, Wetzlar, Germany), and storage in phosphate-buffered saline (PBS).

Selective labeling of mitral cells by viral injection

Some mice were used for fluorescent labeling of individual mitral cells with Sindbis viral vectors. After the mice were deeply anesthetized, Sindbis viral vectors expressing palmitoylation site-attached green fluorescent protein (palGFP, 0.13×10^{10} IU/ml) or

monomeric red fluorescent protein (palmRFP, 0.67×10^{10} IU/ml) (kindly gifted from Drs. Takeshi Kaneko and Takahiro Furuta of Kyoto University; Furuta et al., 2001; Suzuki et al., 2015) in 1 µl of PBS containing 0.5% bovine serum albumin (BSA) were stereotaxically injected into the mitral cell layer of the OB (4.3 mm anterior to bregma, 0.4 mm lateral to midline, and 1.6 mm deep from the brain surface) using a Hamilton syringe (3005FN, Norgren Kloehn, Las Vegas, NV, USA). After 48 hours, the mice were anesthetized and perfused with fixative.

Immunocytochemistry

Sections that included individual mitral cells or accidentally labeled tufted cells were incubated in blocking solution containing 1% BSA and 0.5% sodium azide in PBS for 1 hour at 20°C. Sections were incubated in combinations of fewer than four of the following primary antibodies for 5–7 days at 20°C. Primary antibodies used in this study were as follows: (1) chicken anti-GFP IgY (1:10,000, Life Technologies, Carlsbad, CA, USA, A10262, RRID:AB_11180610); (2) guinea-pig anti-mRFP IgG (1:5000, Kyoto University; Hioki et al., 2010; mRFP1 Guinea, RRID:AB_2336890); (3) mouse anti-vesicular glutamate transporter 1 (VGLUT1) IgG (1:1000, Synaptic Systems, Göttingen, Germany, 135 311, RRID:AB_2187695); (4) rabbit anti-vesicular GABA transporter (VGAT) IgG (1:5000, Millipore, Billerica, MA, USA, AB5062P, RRID:AB_2301998); (5) goat anti-PV IgG (1:5000, Swant, Marly, Switzerland PVG-214, RRID:AB_10000345); and (6) mouse anti-gephyrin (1:5000, Synaptic Systems, 147 011, RRID:AB_887717). After rinsing with PBS, the sections were incubated in biotinylated donkey anti-chicken IgY (1:200, Jackson ImmunoResearch, West Grove, PA, USA, 703-065-155, RRID:AB_2313596) or biotinylated donkey anti-guinea pig IgG (1:200, Jackson ImmunoResearch, 706-065-148,

RRID:AB_2341097) for 2 hours at 20°C and incubated in mixtures containing fluorescent secondary antibodies diluted to 1:200 for 2 hours at 20°C. Secondary antibodies used in this study were as follows: (1) Alexa 488-conjugated streptavidin (Life Technologies, S11223, RRID:AB_2336881); (2) Alexa 555-conjugated streptavidin (Life Technologies, S21381, RRID:AB_2307336); (3) Cy3-conjugated donkey anti-mouse IgG (Jackson ImmunoResearch, 715-165-151, RRID:AB_2315777); (4) Cy3-conjugated donkey anti-rabbit IgG (Jackson ImmunoResearch, 711-165-152, RRID:AB_2307443); (5) Cy3-conjugated donkey anti-sheep IgG (Jackson ImmunoResearch, 713-165-147, RRID:AB_2315778); (6) Alexa Fluor 647-conjugated donkey anti-mouse IgG (Jackson ImmunoResearch, 715-605-151, RRID:AB_2336935); (7) Alexa Fluor 647-conjugated donkey anti-rabbit IgG (Jackson ImmunoResearch, 711-605-152, AB_2492288); and (8) DyLight 405-conjugated donkey anti-mouse IgG (715-475-150, RRID:AB_2340839). Sections were rinsed three times in PBS for 10 minutes after each step. Finally, the sections were mounted on glass slides with VECTASHIELD (Vector Laboratories, Burlingame, CA, USA) and cover-slipped. After the slides were analyzed by confocal microscopy, the sections were rinsed in PBS. Subsequently, the sections were incubated in avidin-biotin peroxidase complex (ABC kit, 1:200, Standard Variety, Vector Laboratories) for 2 hours at 20°C. The peroxidase reaction was visualized using 0.05% 3, 3'-diaminobenzidine tetrahydrochloride (DAB) (Dojindo, Kumamoto, Japan), and 0.01% H_2O_2 in Tris buffer (pH 7.6) for 5–10 minutes at room temperature. After the sections were rinsed in PB, the sections were refixed in 3% glutaraldehyde in 0.1M PB for 30 minutes at 4°C, postfixed in 0.5% osmium tetroxide for 30 minutes at 4°C, and washed with H_2O. Then, the sections were dehydrated through an ethanol gradient, infiltrated with propylene oxide, and flat-embedded in Epon-Araldite.

Characterization of primary antibodies

Primary antibodies used in this study are listed in Table 1. The specificity of these antibodies has been verified in previous studies.

The GFP polyclonal antibody was produced against GFP isolated from jellyfish *Aequorea victoria*, and the IgY fraction was purified by affinity purification. This antibody specifically detected monitored gene expression, and the staining pattern was similar to what was previously reported (Takashima et al., 2007).

The mRFP polyclonal antibody was produced against the full-length coding sequence of mRFP1, which recognized a single 26-kDa protein band on western blot analysis. Immunoreactivity was completely abolished by preincubation of the antibody with an excess amount of antigen protein (Hioki et al., 2010). Specificity of the mRFP antibody was confirmed by the absence of staining in a rat brain that did not receive viral injections (Ito et al., 2015).

The VGLUT1 monoclonal antibody was produced against the Strep-Tag fusion protein containing amino acid residues 456–560 of rat VGLUT1, which recognized a 60-kDa band on western blot analysis. The staining pattern was similar to previous studies (Tafoya et al., 2006; Suñol et al., 2010; Holmseth et al., 2012).

The VGAT polyclonal antibody was produced against a 17-amino acid peptide sequence near the carboxyl terminal region of rat VGAT (VHSLEGLIEAYRTNAED; Mclntire et al., 1997), which recognized a 55–60-kDa band on western blot analysis (Henny and Jones, 2006). Antibody immunoreactivity was blocked by pre-absorption with the antigenic peptide (Rosin et al., 2006). The staining pattern was similar to what was previously reported (Tabuchi et al., 2007).

The PV polyclonal antibody was produced against rat muscle PV, which recognized the 12-kDa band specific for PV (Schwaller et al., 1999) and stained a subpopulation of neurons in the mouse brain with high efficiency (Xu et al., 2010).

Gephyrin is a 93-kDa protein that was co-purified with the glycine receptor (Pfeiffer et al., 1982). The anti-gephyrin monoclonal antibody mAb7a was raised using affinity-purified rat glycine receptors. This antibody does not show immunoreactivity in gephyrin-knockout mice (Feng et al., 1998) and it is widely used to detect gephyrin in symmetrical synapses (Sassoè-Pognetto and Fritschy, 2000). The staining pattern was similar to what was previously reported (Panzanelli et al., 2005).

Electron microscopy

For examination and 3D-reconstruction with EM, the following procedures were conducted. After sections were stained with chicken anti-GFP IgY or guinea-pig anti-mRFP IgG as described above, they were refixed in 3% glutaraldehyde in 0.1 M PB for 30 minutes at 4°C, postfixed in 1% osmium tetroxide for 1 hour at 4°C, and stained in 2% aqueous uranyl acetate for 30 minutes at 4°C. Then, the sections were dehydrated through an ethanol gradient, infiltrated with propylene oxide, flat-embedded in Epon-Araldite, and mounted on blank araldite-cylinders. The samples were cut into 75–80-nm-thick serial thin sections using an ultramicrotome (Reichert-Nissei Ultracut S, Leica) and the sections were then examined using a digital transmission EM (JEM-1400, JEOL, Tokyo, Japan).

Three-dimensional reconstruction of individual mitral cells

(1) Light microscopy: Neurolucida 11.0 software

Individually labeled mitral cells or tufted cells were stained with DAB and flat-embedded

in Epon-Araldite as described above. Each cell was examined in ≤ 12 sections that were 50 µm thick. These cells were digitally traced by light microscopy and 3D-reconstructed using Neurolucida 11.0 software (MBF Bioscience, Colchester, VT, USA, RRID:nif-0000-10294) and a microscope (BX61, ×40/NA 0.94 UPlanSApo objective lens, Olympus, Tokyo, Japan) equipped with a CCD camera (Retiga 2000R, QImaging, British Columbia, Canada).

(2) Correlative analysis of confocal microscopy, Neurolucida, and serial EM

Sections containing individually labeled mitral cells or tufted cells, as described above, were examined by confocal microscopy (A1R-MP, x25/NA 1.1 apochromat objective lens, Nikon, Tokyo, Japan). Serial confocal optical sections were analyzed using a water-immersion objective lens at 0.5-µm intervals. After confocal examination and data recording, mitral cells were 3D-reconstructed using Neurolucida 11.0 software. Then, the sections were processed for EM, cut into serial thin sections, and examined with a digital transmission EM as described above. One mitral cell soma from a female mouse was examined with 5 × 5 montage images covering a 30 × 30-µm area. The primary dendrite and two regions of the secondary dendrite (0–47-µm distance from the soma and 142–210-µm distance from the soma, as calculated using Neurolucida 11.0 software) from another mitral cell of a male mouse were also examined in montages covering areas of 40 × 150 µm, 50 × 30 µm, and 50 × 50 µm, respectively. The dendrite regions were examined in 100–370 serial thin sections. Each image was photographed at a magnification of 4000× (6.3 nm/pixel), where synaptic clefts could be recognized. Mitral cell somata, dendrites, and synaptic distribution were reconstructed and analyzed using Neurolucida 11.0 software. After reconstruction, the examined synapses were individually photographed at a magnification of 20,000× using a digital transmission EM equipped with a tilting

(EM-21311HTR)/rotating (EM-31650SRH31) specimen holder to confirm whether synapses were asymmetrical synapses or symmetrical synapses, and whether mitral cells were presynaptic or postsynaptic. Two regions of the tufted cell secondary dendrites (0–26-μm distance from the soma and 174–270-μm distance from the soma) from another male mouse were also examined in montage images covering areas of 30 × 30 μm of 90 serial-thin sections and 80 × 30 μm of 50 serial-thin sections, respectively, and analyzed using Neurolucida 11.0 software by following the same procedures.

Synapse identification

To establish the confocal method for analyzing synaptic distributions and synaptic relationships with interneurons, sections including labeled mitral cells were multiple-stained with a neuronal marker (PV), and two glutamatergic and GABAergic presynaptic markers (VGLUT1 and VGAT, respectively). Some presumed synapses or neurons observed by confocal microscopy were confirmed by EM.

Sections multiple-stained with the above-mentioned antibody combinations were examined using a confocal microscope (LSM700; ×63/NA 1.4 plan-apochromat oil immersion objective lens, Carl Zeiss, Jena, Germany). Serial optical confocal sections were obtained in 0.3-μm increments and co-localization of mitral cells, neuron markers, and synaptic markers were confirmed. Brightness and contrast were adjusted using ZEN software (Carl Zeiss; RRID:SCR_013672). Some sections were processed for EM, cut with an ultramicrotome into serial-thin sections, and examined using a digital transmission EM, as described above. The regions identified by confocal microscopy were confirmed by EM to include synapses or neuron profiles.

To precisely examine distribution of symmetrical synapses on dendrites of mitral and

tufted cells, sections were multiple-stained with PV, VGAT, and gephyrin (a GABAergic postsynaptic marker) and examined using a confocal microscope (LSM 700) as described above. Imaris 7.7.2 software was used to quantify contact sites between VGAT and gephyrin as putative synaptic sites, and to calculate the dendrite diameter, dendrite surface area, distance from soma, and synaptic densities on the dendrites.

Morphometry

Lengths, diameters, and surface areas of somata or dendrites were analyzed in mitral and tufted cells and using Neuroexplorer 11.0 software (MBF Bioscience), and synaptic densities of each region were calculated by dividing the sum of the number of presynaptic and postsynaptic sites by surface areas. Synaptic distribution was also analyzed using the Sholl analysis (Schmitz et al., 2011; Rotterman et al., 2014); the number of synapses per distance was quantified using a series of concentric circles centered on the origin of a dendrite, and the radius was increased by 10 μm between each circle.

To quantify distributions of secondary dendrites in the EPL, the following methods were used. First, distances were measured vertically from the mitral cell layer (MCL) to the tips of secondary dendrites in the upper region of every section. The EPL width was also calculated by measuring vertically from the MCL to the glomerular layer (GL). Next, the measured distances were calculated as percentages of the EPL width, and the EPL was divided into 10 sublayers from the MCL to the GL. Finally, the percentage of measured points of secondary dendrites distributed within each sublayer was plotted for each cell, and the percentage of tips that belonged to each sublayer was calculated. A total of five mitral cells and five tufted cells were analyzed. This analysis was a technical modification of a previous method (Mori et al., 1983).

Statistical analysis

The difference between synaptic density, as well as the ratio of PV(+) neurons on primary dendrites and secondary dendrites divided by distance from the somata, was assessed between groups using the Student's *t*-test and Welch test. Differences were considered statistically significant at $P < 0.05$. Statistical analysis was performed using StatMate IV software (ATMS Co. Ltd., Tokyo, Japan). Mean ± standard error of mean (S.E.M.) was used for central tendency and dispersion measures.

Results

Morphology of individual mitral cells: general description

Sindbis viral vectors were stereotactically injected into the MCL of the OB in 20 male and nine female mice. A total of 40 mitral cells were fluorescently visualized from 11 male and two female mice, and 13 of them were selected for tracing. A representative example is shown in Figure 1. The mitral cells were identified by the following morphological criteria for somata shape and location, as well as features of dendritic and axonal processes, as previously reported (Price and Powell, 1970; Pinching and Powell, 1971). Single primary dendrites emerged from cell bodies located in the MCL that vertically projected to the GL across the EPL, forming dendritic tufts in the glomerulus. Mitral cells also gave rise to multiple secondary dendrites from somata parallel to the MCL (Figure 1A, B). Virally injected and fluorescently single-labeled mitral cells in the MCL and EPL were subsequently conversion-stained with DAB (Figure 1C) for three-dimensional tracing using Neurolucida software (Figure 1D). Primary dendrites were thick and relatively straight, and had fewer bifurcations than secondary dendrites. Secondary dendrites located in the EPL became thinner as the dendrites extended further from the somata. At least two, although fewer than six, secondary dendrites emerged from the mitral cell body and extended in all directions horizontal to the MCL. The secondary dendrites branched at least twice, but sometimes up to six times, and often spread out further than 1000 μm. Most bifurcated dendrites extended as far as the original dendrites. However, these secondary dendrites did not reach the region superficial to the inner two-thirds of the EPL and were, therefore, typically observed in the deeper EPL region (Figure 2A). Within the inner half of the EPL, the secondary dendrites exhibited various distribution patterns. Some mitral cells were

localized in deeper regions (Mitral cell 1), while others were localized in the middle of the EPL (Mitral cell 5). Compared with mitral cells, other OB projection neurons with somata distributed in the outer half of the EPL, such as tufted cells, were traced using the same methodology. Compared with mitral cells, the dendrites of tufted cells were entirely located in the outer half of the EPL (Figure 2B). Dendrites from these two types of projection neurons were located separately in the EPL (Figure 2).

The morphological characteristics of individual virally labeled mitral cells were consistent with results obtained by Golgi staining or intracellular injections, as described in previous reports (Ramón y Cajal et al., 1904; Mori et al., 1983; Orona et al., 1984). These results suggested that labeling with Sindbis viral vectors was reliable and could be applied to analyses where individual labeling of neurons is required, such as in serial-EM studies.

Synaptic distribution

(1) Somata

The somata of mitral cells were located in the MCL. Cell organelles, such as the nucleus, Golgi apparatus, and rough endoplasmic reticulum, were observed inside the soma and synapses were distributed on the surface of the soma. These features were similar to nearby non-injected mitral cells. The somata had presynaptic sites at asymmetrical synapses and postsynaptic sites at symmetrical synapses, both of which occasionally existed side by side to form reciprocal pairs. These findings generally followed previous reports from random-EM studies (Price and Powell, 1970), which also estimated the number of synapses on the surface of the somata (Benson et al., 1984), although synaptic distribution over the somata or dendrites remains to be analyzed in detail. In the present study, serial sectioning EM-reconstruction studies were performed to determine synaptic distributions on labeled

mitral cells. Initially, cell bodies of mitral cells were examined with special reference to their synapses (Figure 3). Single asymmetrical presynaptic sites that did not form reciprocal pairs (Figure 3B1), single symmetrical postsynaptic sites (Figure 3B2), and reciprocal pairs formed between asymmetrical presynaptic sites and symmetrical postsynaptic sites (Figure 3B3) were observed on the soma (white square in Figure 3A). Neurolucida software was used to show synaptic distribution over the soma (Figure 3B). In total, 290 presynaptic and 217 postsynaptic sites were identified, and the ratio of presynaptic sites to postsynaptic sites was approximately 60%. There were 162 reciprocal pairs, which corresponded with 60% of presynaptic and 80% of postsynaptic sites that formed reciprocal pairs (Figure 6). The soma surface area was 994 μm^2, and the ratio of synapse (asymmetrical presynaptic sites + symmetrical postsynaptic sites) to surface area was 0.51 (synapse/μm^2). These data are summarized in Figure 6. A 3D view of the cell body and synapse (Figure 3B) showed separate synapse-rich and synapse-poor regions. These findings indicate that synaptic distribution on the soma was segregated and could not be estimated without serial-EM studies. Although there were no obvious morphological differences between synapse-poor and synapse-rich areas, glial cells or dendrites from other projection neurons partially covered the surface of the soma, thereby preventing synaptic formation in synapse-poor areas (data not shown).

(2) Secondary dendrites

Serial-sectioning EM was also used to examine two regions of a secondary dendrite of another mitral cell (white square C in Figure 4B; 0-47 μm from the cell body, white square D in Figure 4B; 142–210 μm from the cell body) and their synaptic distribution (Figure 4C, D). There was no fundamental difference in ultrastructure between labeled and non-labeled

dendrites. As observed on the somata, asymmetrical presynaptic sites, symmetrical postsynaptic sites, and reciprocal pairs were found on the secondary dendrites. The diameters of the two region of the secondary dendrite were 2.0–3.7 μm and 1.2–1.9 μm, respectively (Figure 6). Within these two secondary dendrite regions, the ratio of presynaptic to postsynaptic sites was approximately 60%; nearly 60% of presynaptic and 80% of postsynaptic sites were organized into reciprocal pairs (Figure 6). These ratios were similar to the somata and did not change with distance from the somata. The density of synapses, especially synapses distributed far from the somata, was greater than on the somata: the ratio of synapse on secondary dendrites near the somata to surface area and those in the area far from the somata was 1.06 (synapses/μm^2) and 2.51 (synapses/μm^2), respectively (Figure 6). Synaptic segregation was also detected on secondary dendrites (Figure 4C), although synapses in areas far from the somata were more randomly distributed (Figure 4D).

(3) Primary dendrites

Previous studies have shown that primary dendrites are wrapped by glia and have few or no synapses (Shepherd et al., 2004). In this study, however, we found asymmetrical presynaptic sites and symmetrical postsynaptic sites, including reciprocal synapses, which formed between them on the primary dendrites. This apparent contradiction might occur because primary dendrites are sometimes difficult to discriminate from secondary dendrites using random-EM. Synaptic characteristics can be revealed on primary dendrites by serial-EM reconstruction of whole primary dendrites. Thus, we examined all synapses on a primary dendrite, then traced and reconstructed dendrite and synaptic distribution in three dimensions (white square E in Figure 4B, Figure 4E). Total dendrite length was 152 μm,

and the diameter was < 7 μm (2.0–6.5 μm). Similar to other regions examined above, a total of 311 presynaptic sites and 213 postsynaptic sites were identified, and 59% of presynaptic sites and 86% of postsynaptic sites were involved in reciprocal pairs (Figure 6). The ratio of synapse to surface area was 0.51 (synapse/μm^2), which was similar to the ratio in the somata, but less than the ratio on secondary dendrites. These results suggest that synaptic density on primary dendrites is greater than previously believed. Interestingly, the number of synapses on the primary dendrite was less as the dendrites approached the glomerulus (Figure 4E, Figure 5), where synapses were sparsely distributed and glial cells often wrapped the surface of the primary dendrite. Most synapses were distributed in the inner half of the EPL. Conversely, the ratios of asymmetrical presynaptic sites and synapses forming reciprocal pairs were similar to the soma, as well as in two regions of the secondary dendrite. We did not observe postsynaptic sites in asymmetrical synapses in the four analyzed regions.

Correlative study of confocal microscopy and serial-EM using synaptic markers

We confirmed synapse localization by immuno-labeling for presynaptic markers (VGLUT1 and VGAT) and a neuronal marker (PV). Using these markers, synaptic distributions, as determined by serial-EM studies, were confirmed by confocal microscopy. Additionally, synaptic sites, interneuron types forming synapses, and distributions over vast regions were predicted.

We initially compared VGAT(+) sites identified by confocal microscopy with symmetrical synaptic sites identified by EM in four male mice and VGLUT1(+) sites with asymmetrical synaptic sites in five male mice, respectively. A typical example of a mitral cell immuno-labeled for VGLUT1, VGAT, and PV is shown in Figure 7

[GFP(+)/PV(+)/VGAT(+) areas (black arrowhead), GFP(+)/VGAT(+) areas (white arrowhead), and GFP(+)/VGLUT1(+) areas (arrow) in Figure 7A5]. These same areas were examined at a higher resolution using EM (Figure 7B). Direct correlation between confocal microscopic and serial-EM images indicated that asymmetrical synapses (Figure 7B1, arrow) and symmetrical synapses (Figure 7B2-3, arrowhead) were located in VGAT(+) and VGLUT(+) regions, respectively. Symmetrical synapses in Figure 7B2 were formed by PV-immuno-negative (PV(-)) interneurons, and symmetrical synapses in Figure 7B3 were formed by PV(+) neurons. In these regions, 76% of VGAT(+) sites and 84% of VGLUT1(+) sites corresponded to synapses identified by EM [35/46 VGAT(+) sites and 31/37 VGLUT1(+) sites], respectively. Subsequently, immunostaining for GFP, VGLUT1, VGAT, and PV was performed to determine synaptic distribution in five male mice and one female mouse using confocal microscopy. A total of 106 and 89 areas were immuno-positive for VGLUT1 and VGAT, respectively. There were more presumed asymmetrical synapses than symmetrical synapses; 54% of synapses were asymmetrical, which corresponded with serial-EM findings. Additionally, 6.6% of VGLUT1(+) areas and 7.9% of VGAT(+) areas co-localized with PV [7/106 VGLUT1(+) areas, 7/89 VGAT(+) areas, respectively]. These findings were consistent with our previous study of the rat OB (Toida et al., 1996).

Distribution of symmetrical synapses expressing gephyrin

(1) Secondary dendrites

As described above, presynaptic markers were used to estimate synaptic distributions. Gephyrin has been widely used as a GABAergic postsynaptic marker (Hioki et al., 2010; Bartel et al., 2015), and through the combination of VGAT and gephyrin expression,

symmetrical synaptic distribution can be more precisely estimated. Therefore, symmetrical synapse density on secondary dendrites of mitral cells, as well as the variety of interneurons forming synapses with mitral cells, was determined by analyzing protein expression of VGAT, PV, and gephyrin. Examinations were also performed to confirm that tufted cells formed synapses on the outer half of the EPL, at least partially, and to compare tufted cells with mitral cells for analyzing synapse characteristics on mitral cells from many sides. A representative example for GFP, VGAT, PV, and gephyrin immunostaining of a tufted cell is shown in Figure 8. GFP(+)/PV(+)/VGAT(+)/gephyrin(+) areas (white arrow head) were assumed to be symmetrical synapses with PV(+) neurons; GFP(+)/PV(-)/VGAT(+)/gephyrin(+) areas (white arrow) were considered to be symmetrical synapses with non-PV interneurons (granule cells) (Figure 8A5). Symmetrical synapses were quantified on eight mitral cells and eight tufted cells respectively; surface area was measured using Imaris 7.7.2 software, and the density of symmetrical synapses was calculated. These data were divided into three groups according to distance from the somata (0–50 μm, 50–100 μm, and 100–150 μm). Symmetrical synaptic density was distributed on mitral cells from 0.1–0.35 (synapse/μm^2); there was no correlation with distance from the soma (Figure 9A) and no statistical difference between groups (0.192 ± 0.066/μm^2 in 0–50 μm, 0.186 ± 0.043/μm^2 in 50–100 μm, 0.201 ± 0.088/μm^2 in 100–150 μm: 0–50 μm vs. 50–100 μm; P = 0.792, Welch test: 0–50 μm vs. 100–150 μm; P = 0.829, Welch test: 50–100 μm vs. 100–150 μm; P = 0.716, Welch test). As described above, there were 76 symmetrical synapses with a surface area of 172 μm^2 on a region of the secondary dendrite near the mitral cell somata in the serial-EM study. Thus, symmetrical synaptic density in this region of secondary dendrites was 0.44 synapse/μm^2 as determined by EM, which was higher than estimated for this section. Symmetrical synapses were also

identified on secondary dendrites of tufted cells; synaptic density was not different from mitral cells and the density decreased as the dendrites left the somata (Figure 9B). However, there was no statistical difference in synaptic density between the groups of tufted cells (0.226 ± 0.098/μm^2 in 0–50 μm, 0.189 ± 0.047/μm^2 in 50–100 μm, 0.149 ± 0.076/μm^2 in 100–150 μm: 0–50 μm vs. 50–100 μm; P = 0.321, Welch test: 0–50 μm vs. 100–150 μm; P = 0.115, Student's t-test: 50–100 μm vs. 100–150 μm; P = 0.311, Welch test).

The ratio of PV(+) symmetrical synapses was < 25% on each type of cell, and distribution of PV(+) symmetrical synapses on mitral cells was indistinguishable from symmetrical synapses on tufted cells (Figure 10). On tufted cells, there was no statistical difference in the ratio of PV(+) between groups (6.76 ± 7.32% in 0–50 μm, 4.48 ± 6.59% in 50–100 μm, 6.15 ± 4.86% in 100–150 μm: 0–50 μm vs. 50–100 μm; P = 0.562, Student's t-test: 0–50 μm vs. 100–150 μm; P = 0.859, Welch test: 50–100 μm vs. 100–150 μm; P = 0.640, Student's t-test). Compared with tufted cells, the ratio of PV(+) symmetrical synapses on mitral cells gradually diminished as dendrites left the somata, although there was no statistical difference in the ratio of PV(+) between groups (Figure 10A: 9.71 ± 8.14% in 0–50 μm, 9.27 ± 8.44% in 50–100 μm, 4.45 ± 5.41% in 100–150 μm: 0–50 μm vs. 50–100 μm; P = 0.903, Student's t-test: 0–50 μm vs. 100–150 μm; P = 0.103, Welch test: 50–100 μm vs. 100–150 μm; P = 0.220, Welch test).

(2) Primary dendrites

Synaptic distribution on mitral cell primary dendrites, as well as types of interneurons that form synapses with mitral cells, was determined on 10 mitral cells using the same procedure to analyze secondary dendrites. Because the primary dendrite length varied, the distance from the somata was calculated as a percentage of the entire length of each

primary dendrite. The synapses were divided into four groups according to distributed percentages (0–25%, 25–50%, 50–75%, and 75–100%), and synaptic densities were analyzed. Synaptic density of symmetrical synapses was low, ranging from 0.058 to 0.22 synapse/μm^2. Two groups near the somata (0–25% and 25–50%) were statistically higher in synaptic density than the other two groups (Figure 11A: 0.148 ± 0.042/μm^2 in 0–25%, 0.165 ± 0.042/μm^2 in 25–50%, 0.100 ± 0.034/μm^2 in 50–75%, 0.097 ± 0.026/μm^2 in 75–100%: 0–25% vs. 25–50%; $P = 0.500$, Student's *t*-test: 0–25% vs. 50–75%; $P = 0.059$, Student's *t*-test: 0–25% vs. 75–100%; $P < 0.01$, Student's *t*-test: 25–50% vs. 50–75%; $P < 0.05$, Student's *t*-test: 25–50% vs. 75–100%; $P < 0.01$, Student's *t*-test: 50–75% vs. 75–100%; $P = 0.841$, Student's *t*-test). These findings were consistent with synaptic distributions on primary dendrites as determined by EM. The ratio of PV(+) symmetrical synapses was < 20%, with no correlation with distributed percentages (Figure 11B: 6.37 ± 4.92% in 0–25%, 5.50 ± 2.59% in 25–50%, 6.27 ± 4.22% in 50–75%, 5.24 ± 7.02% in 75–100%: 0–25% vs. 25–50%; $P = 0.707$, Welch test: 0–25% vs. 50–75%; $P = 0.961$, Welch test: 0–25% vs. 75–100%; $P = 0.507$, Welch test: 25–50% vs. 50–75%; $P = 0.791$, Student's *t*-test: 25–50% vs. 75–100%; $P = 0.814$, Student's *t*-test: 50–75% vs. 75–100%; $P = 0.604$, Welch test).

Comparative distribution of synapses on secondary dendrites of tufted cells

As described above, tufted cells formed synapses with interneurons on their secondary dendrites in the outer half of the EPL. To more precisely compare morphological and functional differences in local circuits between mitral cells and tufted cells, serial-sectioning EM was used to examine the tufted cells (Figure 12). In this study, middle tufted cells, whose cell bodies were located in the superficial two-thirds of the EPL

(Shepherd et al., 2004), were analyzed (Figure 12A). Cell organelles, such as the nucleus, were observed inside the soma; there were no morphological differences between labeled and non-labeled tufted cells (Figure 12B). Two regions of the secondary dendrites (white square C1 in Figure 12C; 0–26 μm from the soma, white square C2 in Figure 12C; 174–270 μm from the soma), corresponded to areas analyzed in the mitral cell; their synaptic distributions (Figure 12C1, C2) were analyzed. These data are described in Table 2. Similar to the mitral cell, the asymmetrical presynaptic sites, symmetrical postsynaptic sites, and reciprocal pairs of tufted cells were identified (Figure 12C1, C2). The ratios of presynaptic to postsynaptic sites were 51% and 56%, respectively, which were similar to mitral cells. Conversely, the percentages of presynaptic sites and postsynaptic sites to form reciprocal synapses were about 80% and 90%, which were greater than in mitral cells (Table 2). In particular, almost all postsynaptic sites on the secondary dendrite region separate from the somata formed reciprocal synapses; the synaptic density of secondary dendrites near the somata was 1.02 (synapse/μm^2) and those of the secondary dendrite region far from the somata was 1.66 (synapse/μm^2) (Table 2). Thus, synapses on secondary dendrites area far from the tufted cell somata were distributed more sparsely than in mitral cells. Synapses on secondary dendrites near the soma exhibited segregated distribution (Figure 12C1), and synaptic segregation in the area far from the soma was less clear (Figure 12C2).

Discussion

Using single neuron tracing in combination with correlative confocal and serial EM analyses, we have revealed for the first time: 1) the precise synaptic distribution of the entire somata of mouse mitral cells in the OB and the entirety of the primary dendrite; 2) the distribution of symmetrical postsynaptic sites, with two types of GABAergic neurons forming reciprocal synapses with mitral cells – PV(+) neurons and PV(-) neurons (primarily consisting of granule cells); and 3) the difference in types of synapses between mitral cells and tufted cells. Our results revealed the existence of synaptic segregation on the somata, primary dendrites, and secondary dendrites of mitral cells and clearly showed that synapses on the primary dendrite are primarily distributed within the inner half of the EPL. Compared with differences between mitral and tufted cells, there were no significant differences in synapse types between different regions of the somata, or between two secondary dendrite or primary dendrite regions in the mitral cells.

1. Methodological considerations

(1) Single-cell labeling

Synaptic distributions on secondary dendrites are difficult to determine without selective labeling of individual neurons, because mitral cells are not reliably distinguishable from tufted cells using standard EM. This is complicated by the fact that mitral cell secondary dendrites intermingle with dendrites from other projection neurons. Recent procedures for injecting individual neurons with Sindbis viral vectors expressing palGFP or palmRFP have been developed and show promise for cellular identification (Furuta et al., 2001; Suzuki et al., 2015). Infection with Sindbis virus is nontoxic until 48 hours after injection (Takahashi et al., 2003), and electrophysiological properties remain substantially unchanged (Marie

and Malenka, 2006). In the present study, the morphology and ultrastructure of virally injected mitral cells in the mouse OB were similar to non-injected mitral cells, which was consistent with previous findings obtained in the rat OB (Price and Powell, 1970; Pinching and Powell, 1971; Toida et al., 1994). Mitral cells have also been successfully single-labeled with other tracers (Mori et al., 1983; Orona et al., 1984. Nagayama et al., 2010; Igarashi et al., 2012). Previous results have shown that the palGFP- or palmRFP-expressing Sindbis viral vector is a superior technique, because it more precisely labels neurons. Because palGFP and/or palmRFP expression occurs just beneath the cell membrane, tracings of neuronal outlines closely resemble Golgi-stained neurons (Moriyoshi et al., 1996). For these reasons, we selected this labeling method. The present study is the first to report individual mitral cells labeled with fluorescent Sindbis viral vectors, and results show that this method reproducibly labels the entire mitral cell cytoplasm in a stable and efficient manner, allowing for precise examination.

(2) Confirmation of synapses: correlative confocal and serial EM studies

VGLUTs and VGAT are synaptic markers that are localized to presynaptic terminals of glutamatergic neurons (Gabellec et al., 2007, Zander et al., 2010) and GABAergic neurons, respectively (Chaudhry et al., 1998; Dumoulin et al., 1999). Among the VGLUT isoforms, VGLUT1 is expressed in the dendrites of projection neurons within the EPL (Gabellec et al., 2007). In the present study, confocal microscopy results confirmed that mouse OB structures that expressed these markers corresponded with synapses identified by EM, suggesting that synaptic distribution could be analyzed without EM by using synaptic markers.

Gephyrin, a GABAergic postsynaptic marker, has been widely used (Hioki et al., 2010;

Bartel et al., 2015) to identify postsynaptic sites of symmetrical synapses in the rat OB (Giustetto et al., 1998). Double-labeling with VGAT and gephyrin allows for more precise analysis of the distribution of symmetrical synapses with confocal microscopy. In this study, the density of symmetrical synapse on mitral cells, as identified by VGAT and gephyrin, was < 0.35 synapse/μm^2, and the density of symmetrical postsynaptic sites on the secondary dendrite area near the soma, as identified by EM, was 0.44 synapse/μm^2. This difference could be because more than two symmetrical synapses are often adjacent to each other on the same neuronal profile, and these synapses are regarded as one synapse.Most VGAT(+) or VGLUT1(+) regions were PV(-), and the ratio of symmetrical synapses from PV(+) neurons onto mitral cells, as estimated by VGAT and gephyrin expression, was also low. These results were consistent with our previous findings in the rat OB (Toida et al., 1994, 1996) and indicated that this method was reliable.

2. Unique synapse distribution

Synapses on mitral cells were not uniformly distributed, and these findings corresponded with previous studies (Bartel et al., 2015) reporting that synapses identified by gephyrin-immunoreactivity were not uniformly distributed along secondary dendrites of projection neurons (mitral cells or tufted cells). In this study, synaptic segregation was observed on the somata, the region of secondary dendrites near the somata, and on the primary dendrites. Although differences in synaptic formation between synapse-poor areas and synapse-rich areas were not apparent, synapse-poor regions on the mitral cell surface were often covered by glial cells or dendrites from other projection neurons. Interneurons turn over rapidly within a matter of days and may try to establish synapses, but this might be prevented by these covering elements. Thus, synaptic distribution on mitral cells may be

influenced by interneuron turnover (Bartel et al., 2015), as well as surrounding tissues and the mitral cell microenvironment.

Synaptic segregation was more dominant on the somata than on secondary dendrites, and segregation decreased as the dendrites projected further away from the somata. Subgroups of granule cells form selective synapses with the somata of mitral cells (Naritsuka et al., 2009), which could contribute to the unique synaptic segregation on the somata. Conversely, synaptic density on primary dendrites decreased as dendrites approached the glomerulus. The difference in synaptic distribution between primary dendrites and other regions could be related to the dendrite direction. For instance, only primary dendrites passed through the EPL.

Compared with mitral cells, synaptic distribution on tufted cell secondary dendrites was also analyzed. Serial-EM analysis showed that synaptic density on a secondary dendrite area near the somata of tufted cells was similar to mitral cells. Conversely, synapse density on a secondary dendrite area far from the somata of the tufted cell was less than in mitral cells. Confocal laser microscopy used to visualize VGAT and gephyrin showed that synaptic density on tufted cell secondary dendrites decreased as the dendrites left the soma. However, in mitral cells, the synaptic density remained relatively constant, although there were no significant differences between mitral cells and tufted cells. These results imply that compared with tufted cells, synaptic density on mitral cell secondary dendrites increases as dendrites leave the soma. Because newly born granule cells in adult animals are liable to extend their dendrites deep into the EPL (Mandairon et al., 2006; Kelsch et al., 2007), synapses are more continuously and frequently formed on mitral cells than on tufted cells. This could be related to differences in synaptic distribution between mitral cells and tufted cells. Taken together, synaptic distribution on mitral cells is influenced by dendrite

localization, adjacent projection neurons, glial cells, and interneuron subtypes that form synapses.

3. Functional implications

In the EPL, two types of GABAergic interneurons, i.e., granule cells and PV(+) neurons, make contact with projection neurons, form synapses with them, and regulate information transferred to the olfactory cortex (Toida et al., 1996; Toida 2008). Granule cells contact several projection neurons and form reciprocal synapses with a higher probability than PV(+) neurons (Toida et al., 1994; Toida et al., 1996). Granule cells also appear to act preferentially to block propagation of information by recurrent inhibition. Conversely, PV(+) neurons make contact with many projection neurons and have a broad range of olfactory receptive fields (Kato et al., 2013; Miyamichi et al., 2013). PV(+) neurons usually form serial synapses, which consist of two synapses—an asymmetrical synapse from a projection neuron to PV(+) neurons and a symmetrical synapse from PV(+) neurons to other projection neurons—and inhibit adjacent projection neurons via lateral inhibition (Toida et al., 1996; Toida 2008).

As described above, the ratio of symmetrical synapses formed with PV(+) neurons and secondary dendrites decreased as the dendrites moved away from the mitral cell somata. However, the ratio of PV(+) neurons on primary dendrites remained unchanged as dendrites left the somata. Thus, lateral inhibition was more effective in secondary dendrite area near the somata and remained unchanged through the primary dendrites. The projection neuron somata extends the primary dendrites to the same glomerulus and is distributed within a 200-μm radius from the glomerulus. Mitral cells, which are horizontally separated from each other, express different odor selectivity, even though they extend primary dendrites

into the same glomerulus (Kikuta et al., 2013). Precise modifications, such as lateral inhibition near the somata, may be responsible for differences in odor selectivity. Taken together, PV(+) neurons are preferentially distributed on secondary dendrites near the somata, which might be an effective strategy for processing various odor information. Conversely, PV(+) neurons on primary dendrites might be diffusely distributed, because primary dendrites vertically extend to the layers and are not influenced by their horizontal location.

The EPL has been subdivided into two anatomically and functionally distinct sublayers - the inner half and outer half (Mori et al., 1983; Mizuguchi et al., 2012)—because of difference in types of distributed projection neurons (Orona et al., 1984) and granule cells (Mori et al., 1983), as well as PV(+) neuronal density (Kosaka et al., 1994). Tufted cells, mainly distributed in the outer half of the EPL, exhibit a lower threshold to induce spike discharges (Igarashi et al., 2012; Kikuta et al., 2013), a higher firing frequency (Nagayama et al., 2004), and a broader range of olfactory receptive fields (Nagayama et al., 2004; Kikuta et al., 2013) than mitral cells. In this study, asymmetrical presynaptic sites and symmetrical postsynaptic sites on mitral cells formed reciprocal pairs less frequently than on tufted cells. As described above, synapses that form reciprocal pairs act as recurrent inhibition. Conversely, single synapses, which do not form reciprocal pairs, help regulate adjacent projection neurons via interneurons, such as PV(+) neurons. Thus, lateral inhibition of mitral cells predominates over recurrent inhibition. In addition to heterogeneous distribution of PV(+) neurons on secondary dendrites, the lower ratio of reciprocal synapses contributes to higher odor selectivity in mitral cells. Conversely, the smaller quantity of lateral inhibition on tufted cells generates, at least partially, a broader range of a receptive field; the larger quantity of recurrent inhibition may act to control

excessive back-propagation of impulse from excitable tufted cells. Therefore, specific synaptic formations contribute to different functional roles for each projection neurons.

Specific synaptic distribution on mitral cell primary dendrites also plays a role in the construction of local circuits for precise information processing. Synapses on mitral cell primary dendrites are mainly restricted to the inner half of the EPL and secondary dendrites of mitral cells and tufted cells are localized to each sublayer of the EPL. Therefore, local circuits that formed with mitral cells and tufted cells were separated to the inner half and outer half of the EPL, respectively, and efficiently control information in accordance with their different roles (Figure 13).

4. Future studies

Subtypes of mitral cells and tufted cells exist. The internal tufted cells are located in the deep portion of the EPL and extend their secondary dendrites into the intermediate and superficial EPL (Orona et al., 1984). Some mitral cells also extend their secondary dendrites into the superficial EPL (Imamura et al., 2015). To confirm whether segregation of synapses on primary dendrites was related to distribution of secondary dendrites or location of the cell body, and whether local circuits on projection neurons were generally restricted to the EPL sublayer, further studies are needed to analyze synaptic distributions on primary dendrites of these cells.

Conclusions

Using correlative confocal microscopy and serial-EM analyses of individually labeled neurons, we reveal for the first time that synapses on primary dendrites are located primarily in the inner half of the EPL. Additionally, the ratio of synapses to form reciprocal

pairs on mitral cells was less than on tufted cells. Moreover, PV(+) neurons on mitral cell secondary dendrites were frequently distributed near the somata. These results indicate that local synaptic circuits formed on mitral cells are segregated from tufted cells (Figure 13) and suitably composed according to their functional roles.

Acknowledgements

We thank Dr. Peter Baluk of the Department of Anatomy, University of California, San Francisco, for critically reading the manuscript; Prof. Takeshi Kaneko and Dr. Takahiro Furuta of Kyoto University for providing palGFP and palmRFP Sindbis viral vectors, and Ms. Masumi Suda and Ms. Rie Ohmori of the Department of Anatomy, Mr. Taiji Suda and Mr. Nobuaki Matsuda of the Bioimaging Research Unit of the Central Research Institute of Kawasaki Medical School for their technical assistance. This work was supported by MEXT/JSPS KAKENHI Grant Numbers JP15K06748, JP24500418, JP23500419.

Conflict of interest

All authors do not have any conflicts of interest.

Role of authors

All authors had full access to all data in the study and take responsibility for the integrity of the data and accuracy of the data analysis. Study concept and design: Kazunori Toida. Acquisition of data: Takeshi Matsuno. Analysis and interpretation of data: Takeshi Matsuno, Emi Kiyokage, and Kazunori Toida. Drafting of the manuscript: Takeshi Matsuno. Critical revision of the manuscript for important intellectual content: Emi Kiyokage and Kazunori Toida. Obtained funding: Takeshi Matsuno, Emi Kiyokage and Kazunori Toida. Administrative, technical, and material support: Kazunori Toida and Emi Kiyokage. Study supervision: Kazunori Toida.

Literature Cited

Aungst JL, Heyward PM, Puche AC, Karnup SV, Hayar A, Szabo G, Shipley MT. 2003. Centre-surround inhibition among olfactory bulb glomeruli. Nature. 426:623-629.

Bartel DL, Rela L, Hsieh L, Greer CA. 2015. Dendrodendritic synapses in the mouse olfactory bulb external plexiform layer. J Comp Neurol. 523:1145-1161.

Benson TE, Ryugo DK, Hinds JW. 1984. Effects of sensory deprivation on the developing mouse olfactory system: a light and electron microscopic, morphometric analysis. J Neurosci. 4:638-653.

Chaudhry FA, Reimer RJ, Bellocchio EE, Danbolt NC, Osen KK, Edwards RH, Storm-Mathisen J. 1998. The vesicular GABA transporter, VGAT, localizes to synaptic vesicles in sets of glycinergic as well as GABAergic neurons. J Neurosci. 18:9733-9750.

Dumoulin A, Rostaing P, Bedet C, Lévi S, Isambert MF, Henry JP, Triller A, Gasnier B. 1999. Presence of the vesicular inhibitory amino acid transporter in GABAergic and glycinergic synaptic terminal boutons. J Cell Sci. 112:811-823.

Feng G, Tintrup H, Kirsch J, Nichol MC, Kuhse J, Betz H, Sanes JR. 1998. Dual requirement for gephyrin in glycine receptor clustering and molybdoenzyme activity. Science 282:1321-1324.

Furuta T, Tomioka R, Taki K, Nakamura K, Tamamaki N, Kaneko T. 2001. In vivo transduction of central neurons using recombinant Sindbis virus: Golgi-like labeling of

dendrites and axons with membrane-targeted fluorescent proteins. J Histochem Cytochem. 49:1497-1508.

Gabellec MM, Panzanelli P, Sassoè-Pognetto M, Lledo PM. 2007. Synapse-specific localization of vesicular glutamate transporters in the rat olfactory bulb. Eur J Neurosci. 25:1373-1383.

Giustetto M, Kirsch J, Fritschy JM, Cantino D, Sassoè-Pognetto M. 1998. Localization of the clustering protein gephyrin at GABAergic synapses in the main olfactory bulb of the rat. J Comp Neurol. 395:231-244.

Henny P, Jones BE. 2006. Innervation of orexin/hypocretin neurons by GABAergic, glutamatergic or cholinergic basal forebrain terminals evidenced by immunostaining for presynaptic vesicular transporter and postsynaptic scaffolding proteins. J Comp Neurol. 499:645-661.

Hioki H, Nakamura H, Ma YF, Konno M, Hayakawa T, Nakamura KC, Fujiyama F, Kaneko T. 2010. Vesicular glutamate transporter 3-expressing nonserotonergic projection neurons constitute a subregion in the rat midbrain raphe nuclei. J Comp Neurol. 518:668-686.

Holmseth S, Dehnes Y, Huang YH, Follin-Arbelet VV, Grutle NJ, Mylonakou MN, Plachez C, Zhou Y, Furness DN, Bergles DE, Lehre KP, Danbolt NC. 2012. The density of EAAC1 (EAAT3) glutamate transporters expressed by neurons in the mammalian CNS. J Neurosci.

32:6000-6013.

Igarashi KM, Ieki N, An M, Yamaguchi Y, Nagayama S, Kobayakawa K, Kobayakawa R, Tanifuji M, Sakano H, Chen WR, Mori K. 2012. Parallel mitral and tufted cell pathways route distinct odor information to different targets in the olfactory cortex. J Neurosci. 32:7970-7985.

Imamura G, Greer CA. 2015. Segregated labeling of olfactory bulb projection neurons based on their birthdates. Eur J Neurosci. 41:147-156.

Ito T, Hioki H, Sohn J, Okamoto S, Kaneko T, Iino S, Oliver DL. 2015. Convergence of Lemniscal and Local Excitatory Inputs on Large GABAergic Tectothalamic Neurons. J Comp Neurol. 523:2277-2296.

Kato HK, Gillet SN, Peters AJ, Isaacson JS, Komiyama T. 2013. Parvalbumin-expressing interneurons linearly control olfactory bulb output. Neuron. 80:1218-1231.

Kelsch W, Mosley CP, Lin CW, Lois C. 2007. Distinct mammalian precursors are committed to generate neurons with defined dendritic projection patterns. PLoS Biol. 5:e300.

Kikuta S, Fletcher ML, Homma R, Yamasoba T, Nagayama S. 2013. Odorant response properties of individual neurons in an olfactory glomerular module. Neuron. 77:1122-1135

Kosaka K, Heizmann CW, Kosaka T. 1994. Calcium-binding protein parvalbumin-immunoreactive neurons in the rat olfactory bulb. 2. Postnatal development. Exp Brain Res. 99:205-213.

Kosaka K, Aika Y, Toida K, Heizmann CW, Hunziker W, Jacobowitz DM, Nagatsu I, Streit P, Visser TJ, Kosaka T. 1995. Chemically defined neuron groups and their subpopulations in the glomerular layer of the rat main olfactory bulb. Neurosci Res. 23:73-88.

Kosaka K, Toida K, Margolis FL, Kosaka T. 1997. Chemically defined neuron groups and their subpopulations in the glomerular layer of the rat main olfactory bulb--II. Prominent differences in the intraglomerular dendritic arborization and their relationship to olfactory nerve terminals. Neuroscience. 76:775-786.

Lledo PM, Merkle FT, Alvarez-Buylla A. 2008. Origin and function of olfactory bulb interneuron diversity. Trends Neurosci. 31:392-400.

Mandairon N, Sacquet J, Jourdan F, Didier A. 2006. Long-term fate and distribution of newborn cells in the adult mouse olfactory bulb: Influences of olfactory deprivation. 141:443-451.

Marie H, Malenka RC. 2006. Acute in vivo expression of recombinant proteins in rat brain using sindbis virus. In Kittler JT, Moss SJ (ed): The Dynamic Synapse: Molecular Methods in Ionotropic Receptor Biology. Boca Raton: CRC Press. Chapter 12.

Mclntire SL, Reimer RJ, Schuske K, Edfwards RH, Jorgensen EM. 1997. Identification and characterization of the vesicular GABA transporter. Nature. 389:870-6.

Miyamichi K, Shlomai-Fuchs Y, Shu M, Weissbourd BC, Luo L, Mizrahi A. 2013. Dissecting local circuits: parvalbumin interneurons underlie broad feedback control of olfactory bulb output. Neuron 80:1232-1245.

Mizuguchi R, Naritsuka H, Mori K, Yoshihara Y. 2012. Tbr2 deficiency in mitral and tufted cells disrupts excitatory-inhibitory balance of neural circuitry in the mouse olfactory bulb. J Neurosci. 32:8831-8844

Mori K, Kishi K, Ojima H. 1983. Distribution of dendrites of mitral cells, displaced mitral, tufted, and granule cells in the rabbit olfactory bulb. J Comp Neurol. 219:339-355

Mori K, Nagao H, Yoshihara Y. 1999. The olfactory bulb; coding and processing of odor molecule information. Science. 286:711-715.

Moriyoshi K, Richards LJ, Akazawa C, O'Leary DD, Nakanishi S. 1996. Labeling neural cells using adenoviral gene transfer of membrane-targeted GFP. Neuron. 16:255-260.

Nagayama S, Takahashi YK, Yoshihara Y, Mori K. 2004. Mitral and tufted cells differ in the decoding manner of odor maps in the rat olfactory bulb. J Neurophysiol. 91:2532-2540.

Nagayama S, Enerva A, Fletcher ML, Masurkar AV, Igarashi KM, Mori K, Chen WR. 2010.

Differential axonal projection of mitral and tufted cells in the mouse main olfactory system. Front Neural Circuits. 4:120, pii.

Naritsuka H, Sakai K, Hashikawa T, Mori K, Yamaguchi M. 2009. Perisomatic-targeting granule cells in the mouse olfactory bulb. J Comp Neurol. 515:409-426.

Orona E, Rainer EC, Scott JW. 1984. Dendritic and axonal organization of mitral and tufted cells in the rat olfactory bulb. J Comp Neurol. 226:346-356.

Panzanelli P, Perazzini AZ, Fritschy JM, Sassoè-Pognetto M. 2005. Heterogeneity of gamma-aminobutyric acid type A receptors in mitral and tufted cells of the rat main olfactory bulb. J Comp Neurol. 484:121-131.

Pinching AJ, Powell TPS. 1971 The neuropil of the glomeruli of the olfactory bulb. 1971. J Cell Sci. 9;347-377.

Price JL, Powell TPS. 1970. The mitral and short axon cells of the olfactory bulb. J Cell Sci. 7:631-51.

Pfeiffer F, Graham D, Betz H. 1982. Purification by affinity chromatography of the glycine receptor of rat spinal cord. J Biol Chem. 257:9389-9393.

Ramón y Cajal S. 1899-1904. Textura del Sistema nervioso del hombre y de los vertebrados.

Madrid: Librería Nicolás Moya. (Swanson N, Swanson LW translator. 1995. Histology of the nervous system of man and vertebrates. New York: Oxford University Press)

Rosin DL, Chang DA, Guyenet PG. 2006. Afferent and efferent connections of the rat retrotrapezoid nucleus. J Comp Neurol. 499:64-89.

Rotterman TM, Nardelli P, Cope TC, Alvarez FJ. 2014. Normal distribution of VGLUT1 synapses on spinal motoneuron dendrites and their reorganization after nerve injury. J Neurosci. 34:3475-3492.

Sassoè-Pognetto M, Fritschy JM. 2000. Mini-review: gephyrin, a major postsynaptic protein of GABAergic synapses. Eur J Neurosci. 12:2205-2210.

Schmitz SK, Hjorth JJ, Joemai RM, Wijntjes R, Eijgenraam S, de Bruijn P, Georgiou C, de Jong AP, van Ooyen A, Verhage M, Cornelisse LN, Toonen RF, Veldkamp WJ. 2011. Automated analysis of neuronal morphology, synapse number and synaptic recruitment. J Neurosci Methods. 195:185-193.

Schwaller B, Dick J, Dhoot G, Carroll S, Vrbova G, Nicotera P, Pette D, Wyss A, Bluethmann H, Hunziker W, Celio MR. 1999. Prolonged contraction-relaxation cycle of fast-twitch muscles in parvalbumin knockout mice. Am J Physiol. 276:C395-403.

Shepherd GM, Chen WR, Greer CA. 2004. Olfactory bulb. In G.M. Shepherd (ed): The Synaptic Organization of the Brain 5th ed. New York: Oxford University Press, pp. 165-216.

Suñol C, Babot Z, Cristòfol R, Sonnewald U, Waagepetersen HS, Schousboe A. 2010. A possible role of the non-GAT1 GABA transporters in transfer of GABA from GABAergic to glutamatergic neurons in mouse cerebellar neuronal cultures. Neurochem Res. 35:1384-1390.

Suzuki Y, Kiyokage E, Sohn J, Hioki H, Toida K. 2015. Structural basis for serotonergic regulation of neural circuits in the mouse olfactory bulb. J Comp Neurol. 523:262-280.

Tabuchi K, Blundell J, Etherton MR, Hammer RE, Liu X, Powell CM, Südhof TC. 2007. A neuroligin-3 mutation implicated in autism increases inhibitory synaptic transmission in mice. Science. 318:71-76.

Tafoya LC, Mameli M, Miyashita T, Guzowski JF, Valenzuela CF & Wilson MC. 2006. Expression and function of SNAP-25 as a universal SNARE component in GABAergic neurons. J Neurosci. 26:7826-7836.

Takahashi T, Svobada K, Malinow R. 2003. Experience strengthening transmission by driving AMPA receptors into synapses. Science. 229:1585-1588

Takashima Y, Daniels RL, Knowlton W, Teng J, Liman ER, McKemy DD. 2007. Diversity in the neural circuitry of cold sensing revealed by genetic axonal labeling of transient receptor potential melastatin 8 neurons. J Neurosci. 27:14147-14157.

Toida K, Kosaka K, Heizmann CZ, Kosaka T. 1994. Synaptic contacts between mitral/tufted cells and GABAergic neurons containing calcium-binding protein parvalbumin in the rat olfactory bulb, with special reference to reciprocal synapses between them. Brain Res. 650:347-352.

Toida K, Kosaka K, Heizmann CZ, Kosaka T. 1996. Electron microscopic serial-sectioning/reconstruction study of parvalbumin-containing neurons in the external plexiform layer of the rat olfactory bulb. Neurosci. 72:449-466.

Toida K. 2008. Synaptic organization of the olfactory bulb based on chemical coding of neurons. Anat Sci Int. 83:207-217.

Xu X, Roby KD, Callaway EM. 2010. Immunochemical characterization of inhibitory mouse cortical neurons: three chemically distinct classes of inhibitory cells. J Comp Neurol. 518:389-404.

Yokoi M, Mori K, Nakanishi S. 1995. Refinement of odor molecule tuning by dendrodendritic synaptic inhibition in the olfactory bulb. Proc Nati Acad Sci U S A 92:3371-3375

Zander JF, Münster-Wandowski A, Brunk I, Pahner I, Gómez-Lira G, Heinemann U, Gutiérrez R, Laube G, Ahnert-Hilger G. 2010. Synaptic and vesicular coexistence of VGLUT and VGAT in selected excitatory and inhibitory synapses. J Neurosci. 30:7634-7645.

Figure legends

Figure 1

Visualization of an individual mitral cell. (A) Mitral cell labeled by Sindbis virus. (B) Soma of labeled cell is located in the MCL, and the dendrite extends across the EPL and forms a dendritic tuft in the glomerulus. (C) Fluorescent labeling is converted to bright-field labeling. (D) 3D-reconstructed mitral cell with dendrites (black) and axon (orange). The secondary dendrites horizontally extend to the MCL. Blue dotted lines indicate borders between each layer. GL, glomerular layer; EPL, external plexiform layer; MCL, mitral cell layer. Scale bar is 500 μm in A; 100 μm in B, C, and D.

Figure 2

Distributions of secondary dendrites in the EPL. EPL is equally divided into 10 sublayers from the MCL toward the GL (I to X respectively). The percentages of secondary dendrites in each sublayer of five mitral cells and five tufted cells are shown. Individual cells are shown in different colors. Dendrites of mitral cells are distributed to the inner half of the EPL, whereas dendrites of tufted cells are in the outer half of the EPL.

Figure 3

Synaptic distribution on the soma. (A) Mitral cell labeled by Sindbis virus. Areas surrounded by white squares were traced and reconstructed. (B) 3D reconstruction of soma from 288 electron microscopic serial-sections. Red dots indicate asymmetrical synapses from the mitral cell (B1), and blue dots represent single symmetrical synapses to a mitral cell (B2). Pink dots indicate asymmetrical synapses of reciprocal pairs, and light blue dots are symmetrical synapses of reciprocal pairs (B3). Arrows and arrowheads indicate an

asymmetrical synapse and symmetrical synapse, respectively. M, mitral cells; GL, glomerular layer; EPL, external plexiform layer; MCL, mitral cell layer; GCL, granule cell layer. Scale bar is 100 μm in A and B1–3; 5 μm in B.

Figure 4

Synaptic distribution on two areas of secondary dendrites and a primary dendrite. (A) Another mitral cell labeled by Sindbis virus. (B) 3D reconstructed mitral cell with dendrites (red) and an axon (green). (C) 3D reconstruction of one secondary dendrite area from the rectangular area C in B. (D) 3D reconstruction of another secondary dendrite area from the white square D in B. (E) 3D reconstruction of a primary dendrite from the white rectangular area E in B. Red dots indicate asymmetrical synapses, and blue dots are symmetrical synapses. Pink dots indicate asymmetrical synapses from reciprocal pairs and light blue dots are symmetrical synapses from reciprocal pairs. GL, glomerular layer; EPL, external plexiform layer; MCL, mitral cell layer; GCL, granule cell layer. Scale bar is 50 μm in A and B; 5 μm in C; 10 μm in D and E.

Figure 5

Graph of synaptic distribution on primary dendrite. Number of presynaptic sites and postsynaptic sites on a primary dendrite; 10-μm increments from the soma are shown. Synaptic density decreases with increasing distance of sampled region from the soma. Correlation coefficient between presynaptic sites and distance is -0.92, with a distance of -0.83 between postsynaptic sites.

Figure 6

Data from four regions analyzed by serial EM studies. Somata and three black rectangular areas were analyzed. Numbers in parentheses describe the percentages of reciprocal pairs to all asymmetrical or symmetrical sites. In all four regions, the ratio of asymmetrical sites to symmetrical sites is 3 to 2. Φ, diameter; A, asymmetrical synaptic sites; S, symmetrical synaptic sites; R, reciprocal pairs; SA, surface area; D, synaptic density.

Figure 7

Combined confocal and serial EM analysis of mitral cells. (A) Confocal projection image of immunolabeled mitral cells (green) and PV (red). Higher magnification of the white rectangle area in A, which was immunostained for GFP (green), PV (red), VGAT (yellow), and VGLUT (magenta), is shown in A1–A5. GFP-positive (GFP+)/PV(+)/VGAT(+) area (black arrowhead), GFP(+)/VGAT(+) area (white arrowhead), and GFP(+)/VGLUT1(+) area (arrow). (B) Electron microscopic image of inset in A. B1–3 shows high magnification from each box in B. A presynaptic site of asymmetrical synapse (B1, arrow), and postsynaptic sites of symmetrical synapses (B2 and 3, arrowhead) on mitral cell in VGLUT1 and VGAT positive areas, respectively. M, mitral cells; VGLUT1, vesicular glutamate transporter; VGAT vesicular gamma-aminobutyric acid transporter; PV, parvalbumin. Scale bar is 20 μm in A; 2 μm in A1–5; 1 μm in B; 200 nm in B1–3.

Figure 8

Distribution of symmetrical synapses on tufted cell dendrites. (A) Confocal projection image of immunolabeled tufted cells (green) and PV (red). Higher magnification of the white rectangle area in A, which was immunostained for GFP (green), PV (red), VGAT (blue), and gephyrin (yellow) shown in A1–A5. VGAT(+)/gephyrin(+) puncta identified as

symmetrical synapses. Dendrites of tufted cells receive symmetrical synapses from PV (arrowhead) and non-PV neurons (arrows), presumed to be granule cells. VGAT, vesicular gamma-aminobutyric acid transporter; PV, parvalbumin. Scale bar is 20 μm in A; 2 μm in A1–5.

Figure 9

Density of symmetrical synapses on secondary dendrites of mitral cells and tufted cells. The density of symmetrical synapses was examined on multiple secondary dendrites of mitral cells or tufted cells and arranged by distance from the somata. Density of all symmetrical synapses onto secondary dendrites of mitral (A) and tufted cells (B). The density of symmetrical synapses onto tufted cells decreases gradually as dendrites extend further from the somata (B). However, there is no statistical difference between groups when distance from the somata was analyzed. PV, parvalbumin. Horizontal bars indicate median values.

Figure 10

Ratio of symmetrical synapses from PV(+) onto dendrites of mitral (A) and tufted cells (B). Compared with findings for symmetrical synapse density on mitral cells, the ratio of symmetrical inputs from PV(+) decreases with distance of dendrites from the somata (A). There are no significant distribution differences of synapses from PV(+) profiles for mitral cells or tufted cells. PV, parvalbumin. Horizontal bars indicate median values.

Figure 11

Density of symmetrical synapse on primary dendrites (A), and the ratio of PV(+) interneurons forming synapses with them (B). Distances from somata were calculated as percentages of the entire length of each primary dendrite. Two groups near the somata (0–25% and 25–50%) are statistically higher in synaptic density than the other two groups, although the ratio of PV(+) profiles does not change with distance from the somata. PV, parvalbumin. Horizontal bars indicate median values. $^{**}P < 0.01$; $^{*}P < 0.05$; in Student's *t*-test.

Figure 12

Synaptic distribution on two secondary dendrite areas of tufted cells as detected by serial-EM. (A) Middle tufted cells were labeled by Sindbis virus and converted to bright-field labeling. (B) Electron micrograph of the same middle tufted cell. (C) 3D reconstructed tufted cell with dendrites (green) and an axon (orange). (C1) 3D reconstruction of one secondary dendrite are from the rectangular area C1 in C. (C2) 3D reconstruction of another secondary dendrite are from the white square C2 in C. Red dots indicate asymmetrical synapses, and blue dots are symmetrical synapses. Pink dots indicate asymmetrical synapses from reciprocal pairs and light blue dots are symmetrical synapses from reciprocal pairs. GL, glomerular layer; EPL, external plexiform layer; MCL, mitral cell layer. Scale bar is 50 μm in A; 20 μm in C; 10 μm in C2; 5 μm in B and C1.

Figure 13

Summary schematic diagram. Local synaptic circuits of mitral and tufted cells are separately distributed within the inner and outer halves of the EPL respectively, and PV(+) neurons preferentially form synapses with mitral cells near their somata. Red arrows

indicate asymmetrical synapses and blue arrows indicate symmetrical synapses. Areas sandwiched between two continuous lines represent the EPL, and the dotted line indicates the boundary between the inner and outer halves of the EPL. GL, glomerular layer; EPL, external plexiform layer; MCL, mitral cell layer; GCL, granule cell layer; PV, parvalbumin.

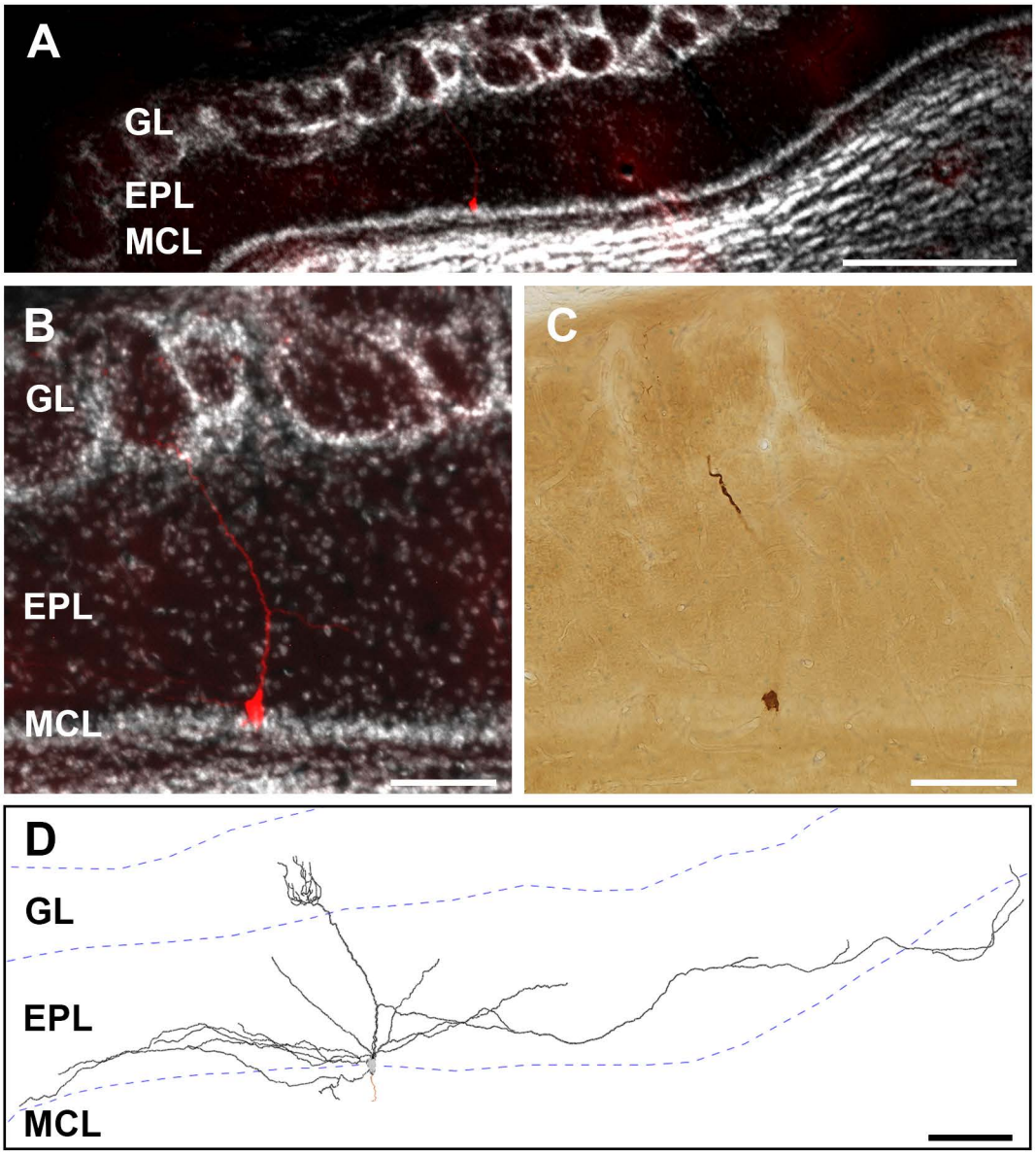

Figure 1 Matsuno et al.

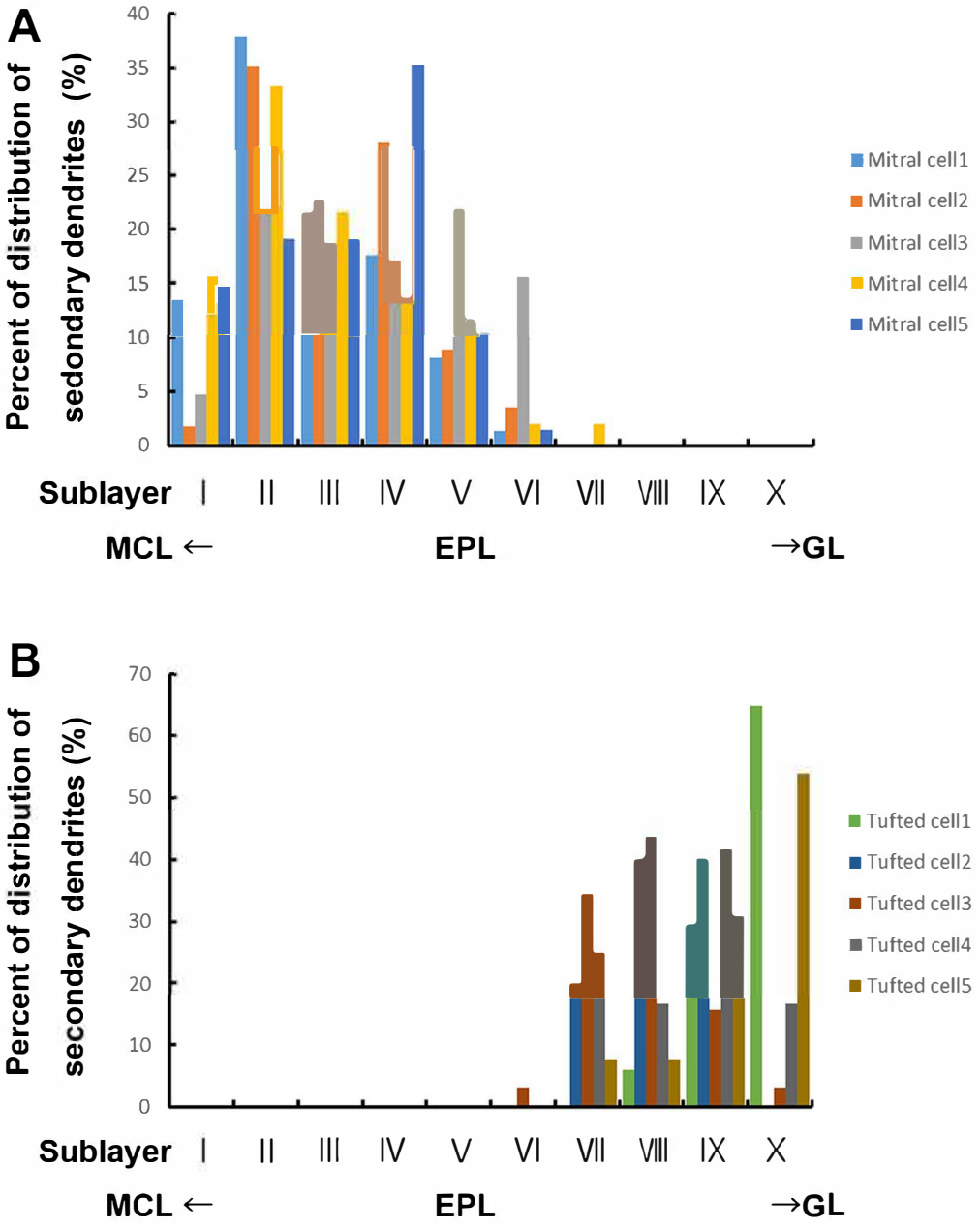

Figure 2 Matsuno et al.

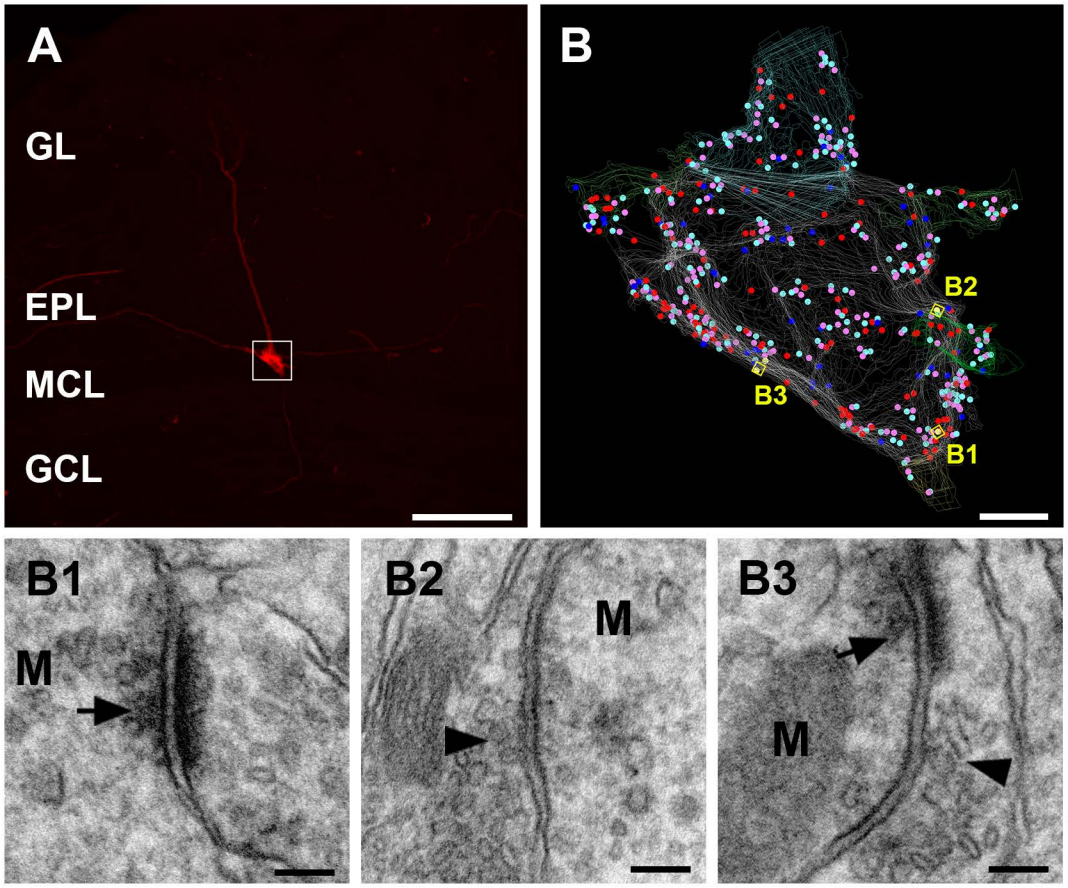

Figure 3 Matsuno et al.

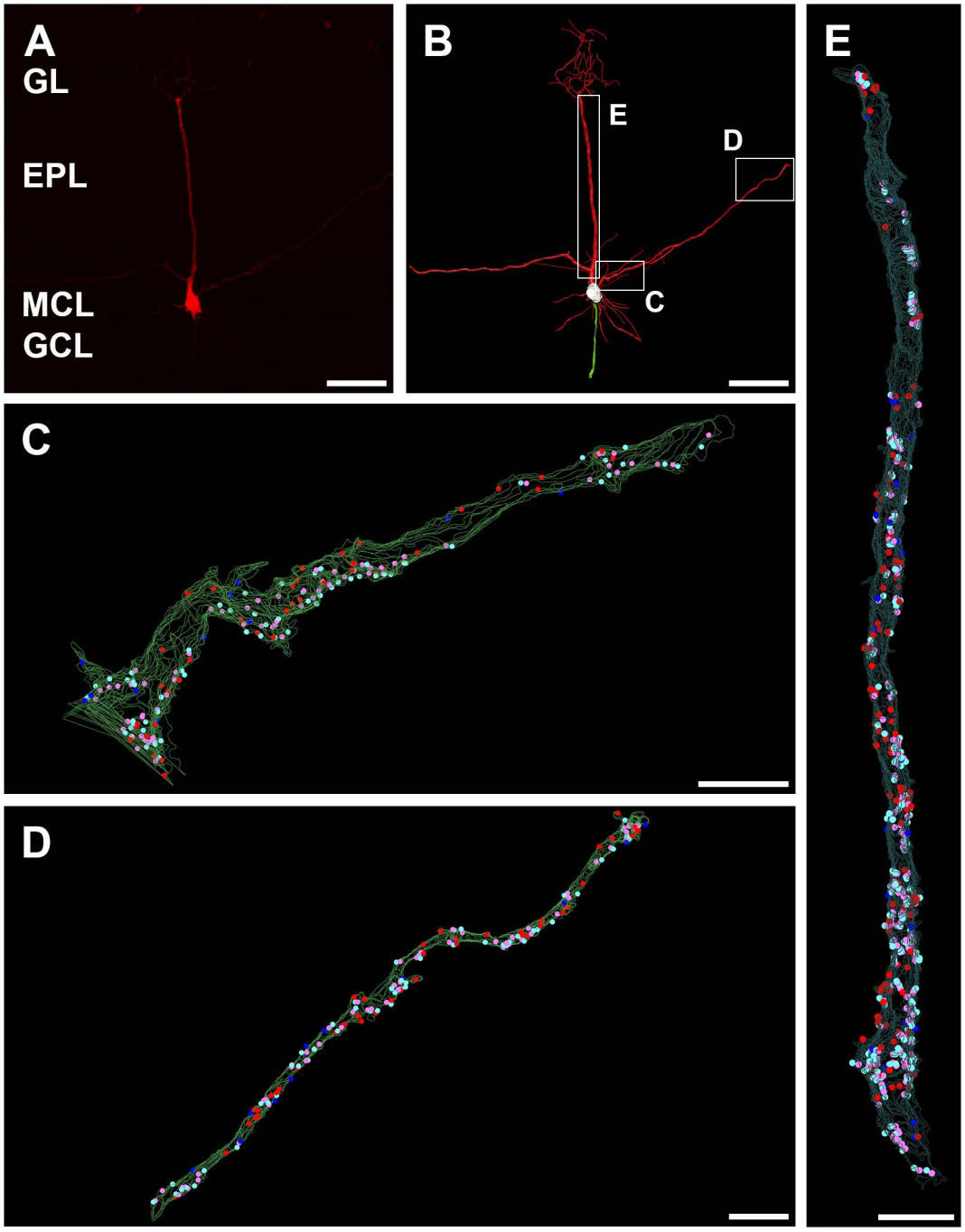

Figure 4 Matsuno et al.

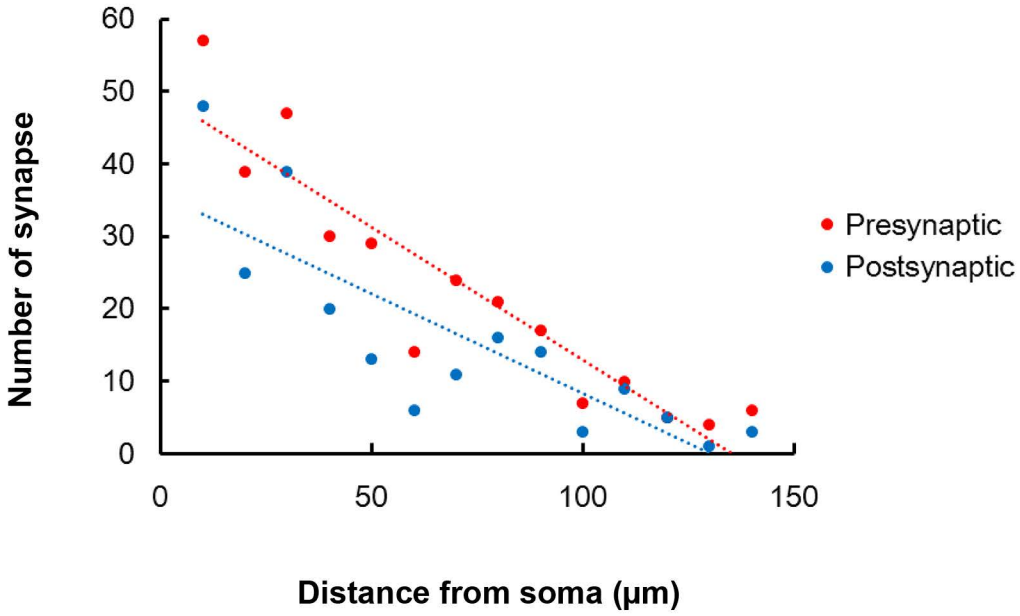

Figure 5 Matsuno et al.

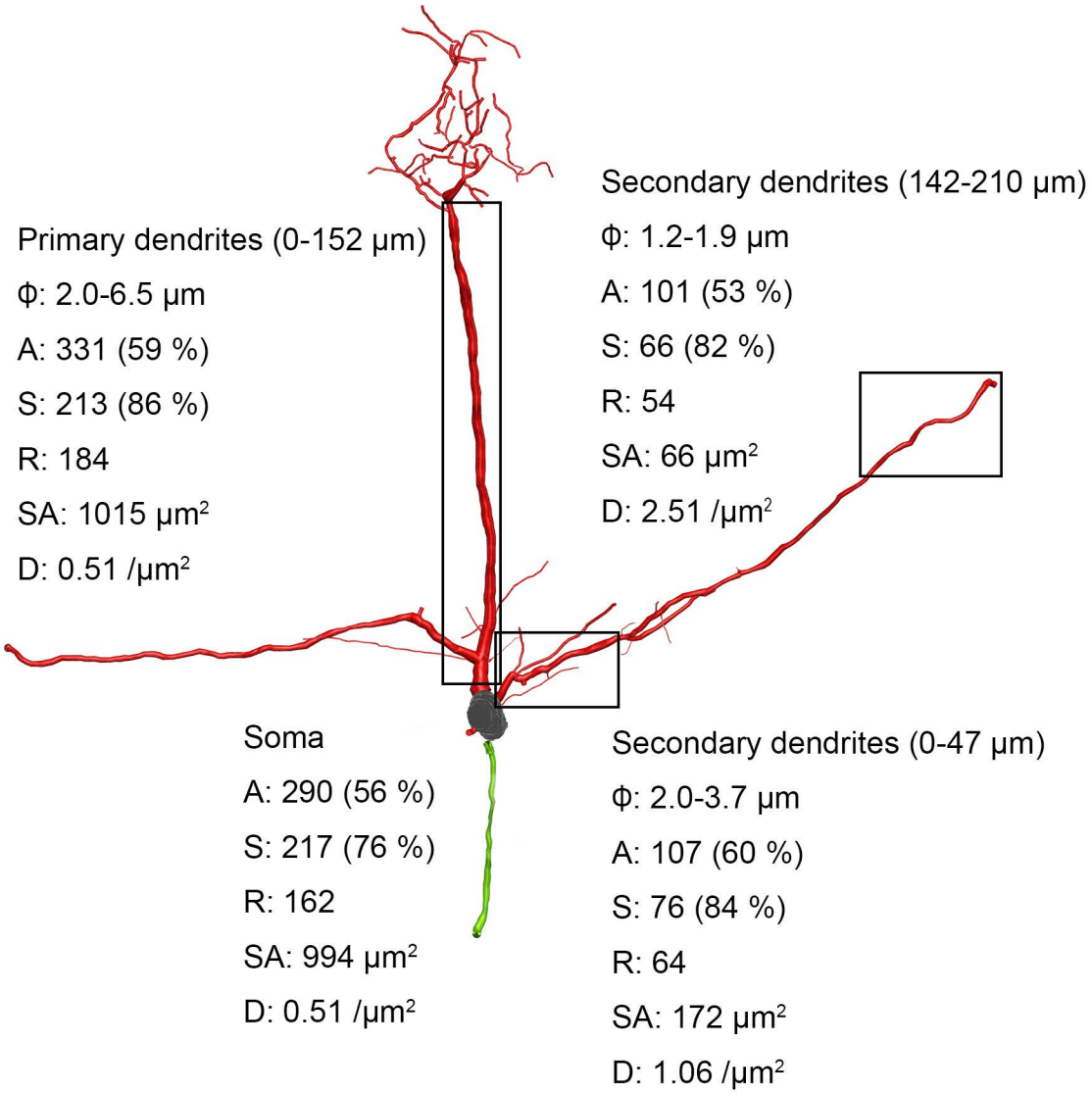

Figure 6 Matsuno et al.

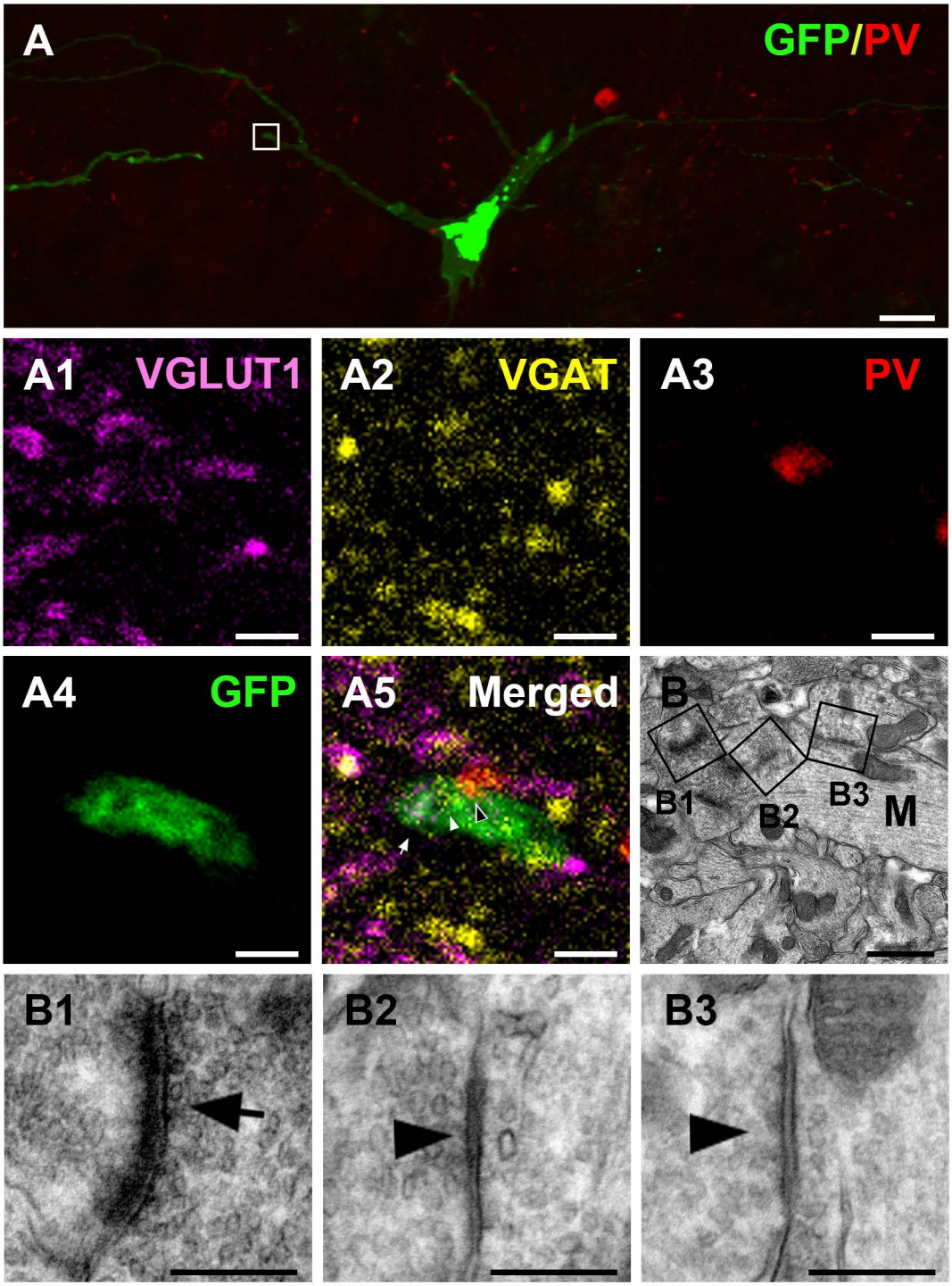

Figure 7 Matsuno et al.

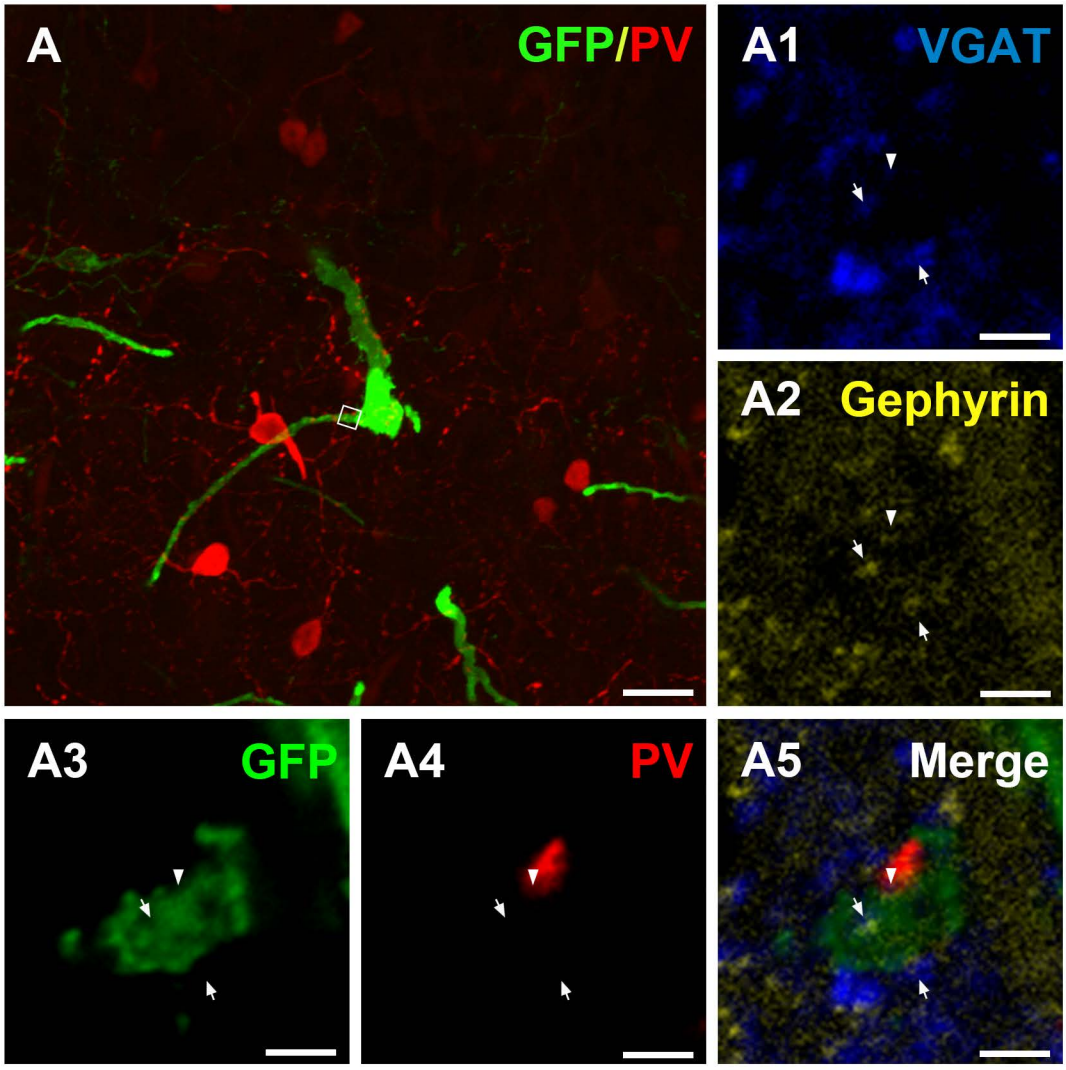

Figure 8 Matsuno et al.

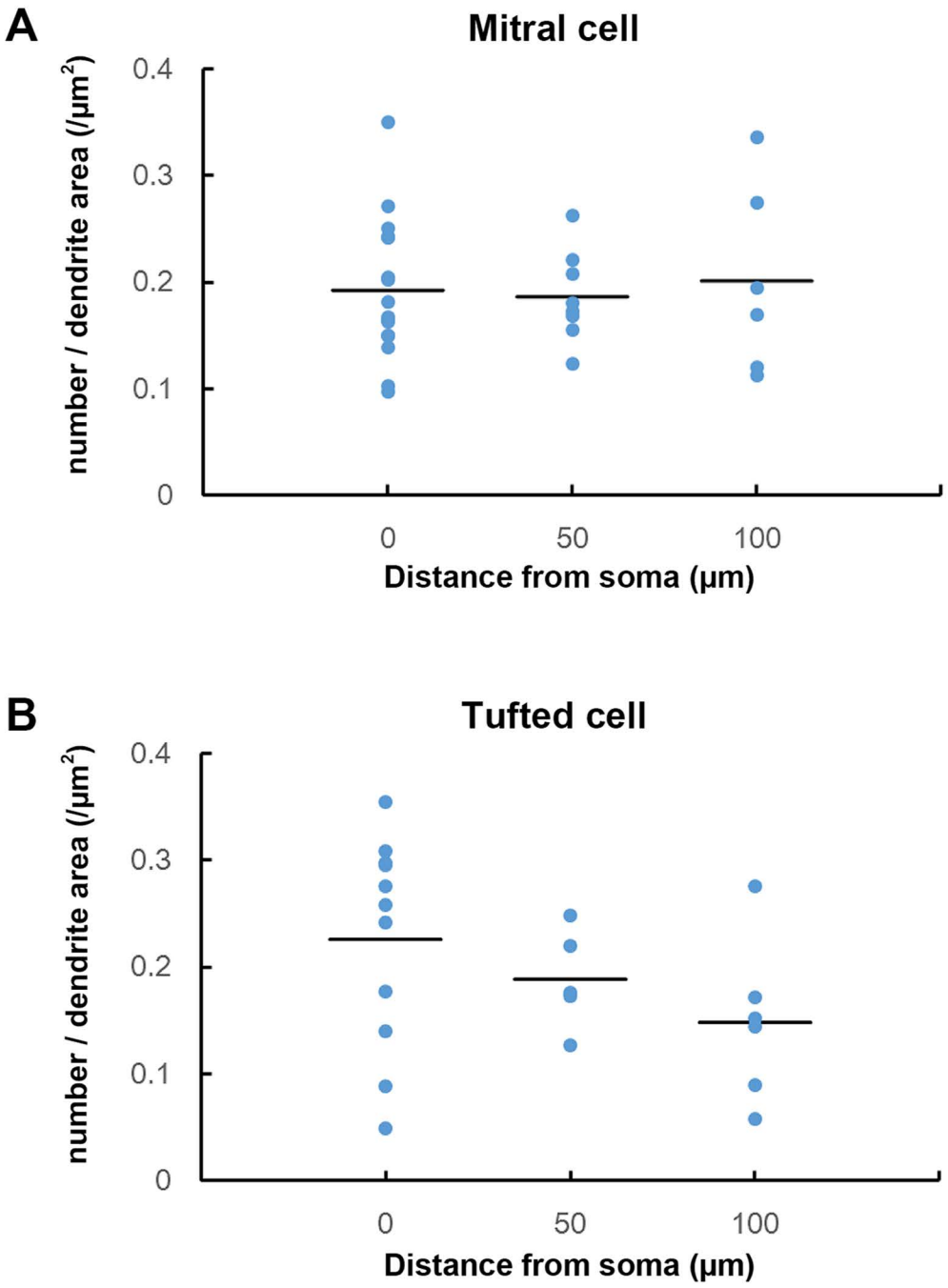

Figure 9 Matsuno et al.

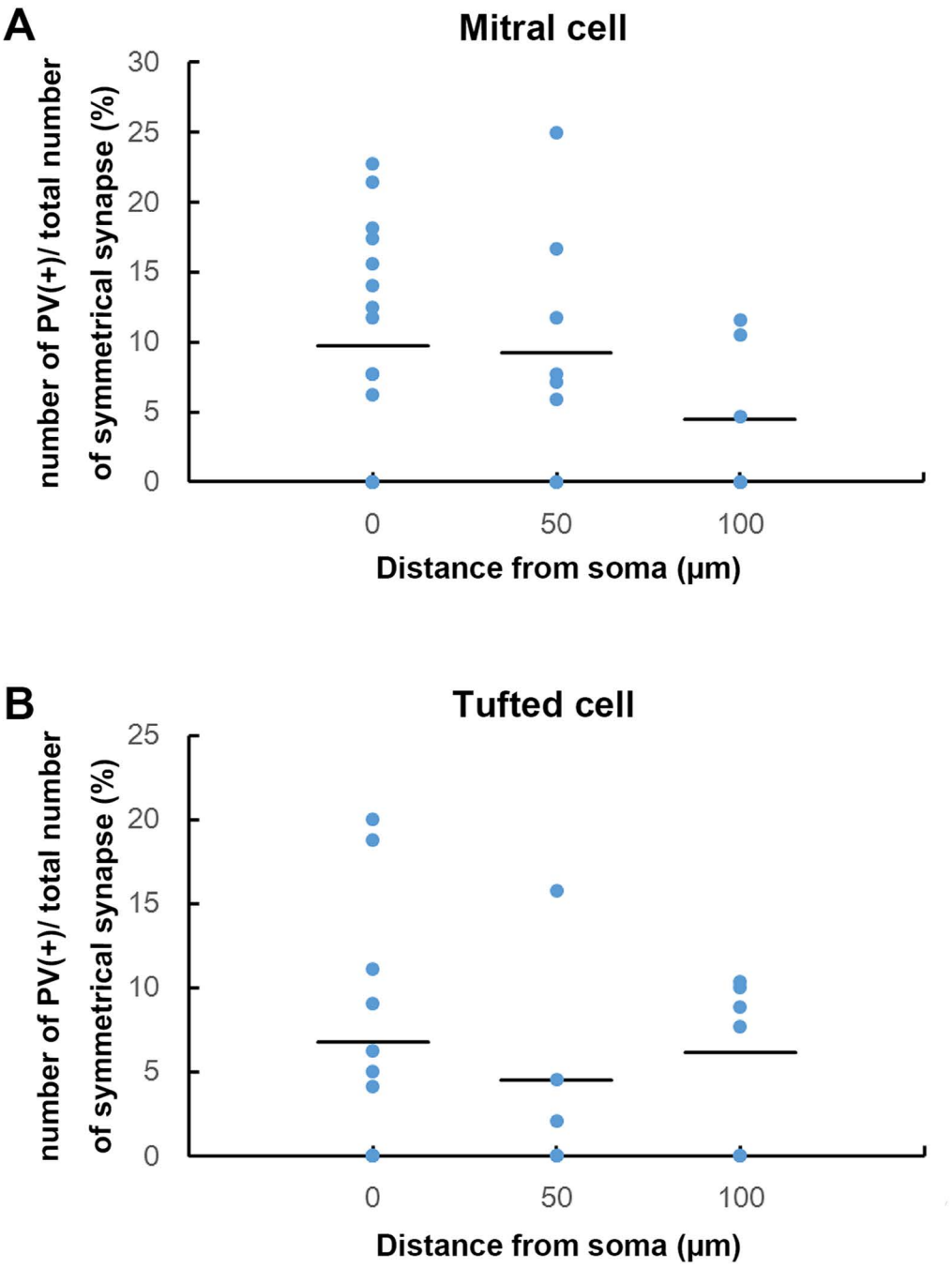

Figure 10 Matsuno et al.

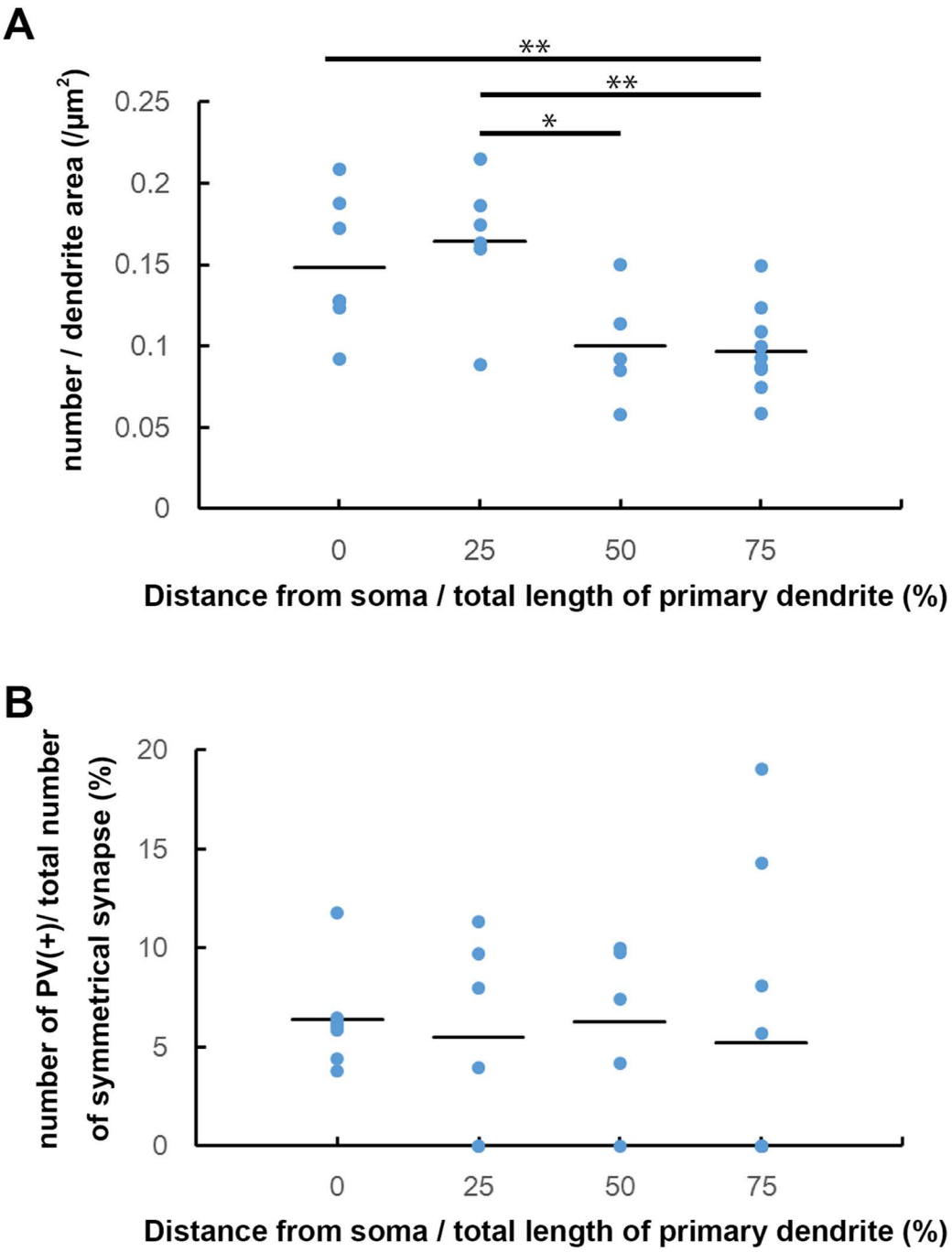

Figure 11 Matsuno et al.

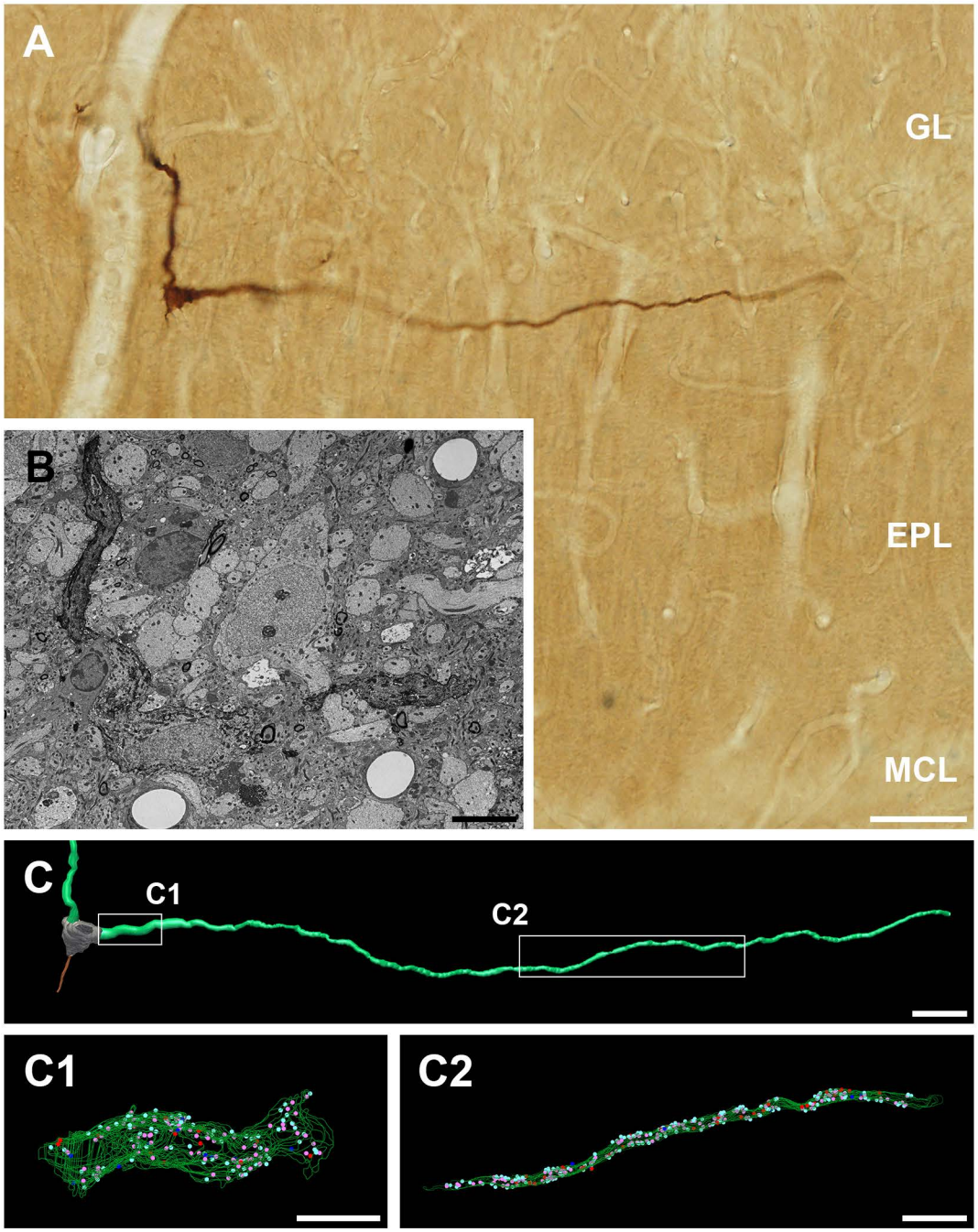

Figure 12 Matsuno et al.

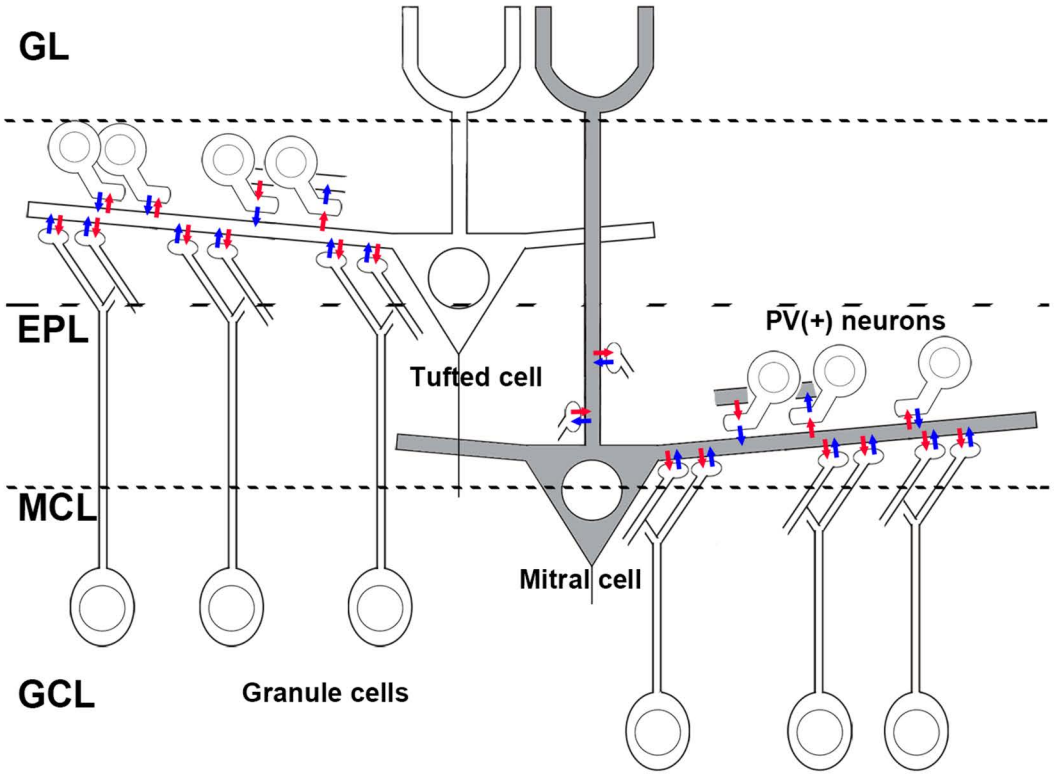

Figure 13 Matsuno et al.

Table 1. Table of Primary Antibodies Used

Antigen	Description	Source, Cat#, Clone or Lot#, RRID, Host Species	Concentration
GFP	Full-length coding sequence of GFP isolated directly from the jellyfish Aequorea victoria	Life Tecnology, Cat# A10262, lot# 1131001, RRID:AB_11180610, chicken polyclonal	1:10000
mRFP	Full-length coding sequence of mRFP1	Kyoto Univ, Cat# mRFP Guinea, RRID:AB_2336890, guinea pig polyclonal	1:5000
VGLUT1	Strep-Tag fusion protein of rat VGLUT1 (aa 456 - 560)	Synaptic systems, Cat# 135 311, Clone 317D5, RRID:AB_2187695, mouse monoclonal	1:1000
VGAT	A 17 amino acid peptide sequence near the carboxy terminal region of rat VGAT (VHSLEGLIEAYRTNAED)	Millipore, Cat# AB5062P, lot# NG1809234, RRID:AB_2301998, rabbit polyclonal	1:5000
Parvalbumin	Rat muscle parvalbumin	Swant, Cat# PVG-214, lot# 3.6, RRID:AB_2313848, goat polyclonal	1:5000
Gephyrin	Reconmbinant fragment (aa 294–736) of rat gephyrin	Synaptic Systems, Cat# 147 011, Clone mAb7a, RRID:AB_887717, mouse monoclonal	1:5000

Table 2. Number and density of synapses from two regions of tufted cell secondary dendrites

Distance from the somata	Diameter (µm)	Number of asymmetrical synapses (Percentage of synapses forming reciprocal paris (%))	Number of symmetrical synapses (percentage of synapses forming reciprocal pairs (%))	Reciprocal pairs	Surface area (μm^2)	Density of synapses (/ μm^2)
0-26 µm	3.6-4.6	101 (84)	96 (89)	85	192.40	1.02
174-270 µm	1.2-2.5	166 (80)	132 (96)	132	183.57	1.66